



CRITICAL CURRENT DEGRADATION IN REBCO AND BI-2223 SUPERCONDUCTORS UNDER TORSIONAL AND TENSILE STRAIN

Jaap Kosse

FACULTY: SCIENCE AND TECHNOLOGY (TNW)
RESEARCH CHAIR: ENERGY, MATERIALS AND SYSTEMS (EMS)

Teacher: Arend Nijhuis
Tutor: Rutger Pompe van Meerdervoort
Coordinator: Stefan Kooij

2013-06-24

Acknowledgements

This bachelor assignment was provided to me by Arend Nijhuis, who let me handle it in a way which gave me a lot of freedom; this was a manner of working which I enjoyed and which allowed me to work in the way I wanted. Guidance from his part helped me towards completing the assignment.

On a daily basis, I worked mostly with Rutger Pompe van Meerdervoort, whose technical skills helped make this assignment possible. At times, watching Rutger at work made me feel like a monkey in a control room in comparison. Thankfully, he patiently transferred at least some technical skills to me during the assignment.

Sander Wessel helped me a lot in learning to work in the lab, and seems to have a niche in fixing in a couple of minutes computer problems which were able to occupy hours of my time trying to fix them myself.

I also want to thank Chao Zhou and Gabriella Rolando, in particular for their help with the COMSOL simulations.

The nice pictures of the Bi-2223 and ReBCO tapes cross-sections were made by Ruben Lubkemann; besides their scientific value, they are also nice to look at.

The whole EMS-research chair provided me with a friendly and laid-back work environment, which enabled me not only to learn a great deal during my assignment, but also to have fun doing so.

Thanks to all!

Summary

Measurements were done on superconducting Bi-2223 and ReBCO tapes, investigating the behaviour of the critical current, I_c , under torsional and tensile strains. For this purpose a new insert was made that would allow these strains to be applied while cooling the samples to 77 K using liquid nitrogen. The new probe will be used for testing different ReBCO tapes from various manufacturers aiming for the selection of the most suitable tape for magnet coils in DEMO, the next nuclear fusion reactor after ITER.

The samples were soldered to copper contacts on the sample holder in order to secure the sample and to provide the current. The sample holder is designed to allow stress-free contraction while cooling down to measurement temperatures.

I_c is determined from measured $I - V$ curves using the standard four probe method. After every measurement the applied strain is removed and a measurement is performed to determine the reversibility of the I_c degradation.

The n -index gives an indication of how the electric field depends on the current in the transition region; it is obtained by fitting measured $I - V$ data to the equation:

$$E = E_c \left(\frac{I}{I_c} \right)^n$$

where E_c is the electric field criterion.

Simulations in COMSOL using the finite element method (FEM) help to provide an understanding of stress profiles in the ReBCO tape resulting from torsional strain, valid in the elastic stress-strain region. From comparing the stress-to-yield stress ratios across the different materials in the tape, it can be concluded that the copper sheets are the first to show plastic deformation, after which a redistribution of stress will occur.

A Bi-2223 tape was measured first to examine if the insert works properly. The torsion test done on this sample showed that this old Bi-2223 tape permanently damages on applying torsional strain, with almost no reversibility observed.

The ReBCO tape used is the SCS4050 tape, manufactured by SuperPower. For the ReBCO tape under strain, the homogeneity of the I_c across taps is good up to the critical strain, ε_c , after which divergent behaviour can be observed. Reversibility is very high until around ε_c , after which it drops sharply. The n -index shows a slow decrease at higher strain which is still present after the strain has been removed.

It is very likely that damage resulting from tensile strain will occur because of the formation of cracks at localized sites, while damage occurring from torsional strain occurs more gradually because cracks can propagate more uniformly along the tape. This explains the more sudden I_c -degradation under tensile strain compared to torsional strain.

For the Nb₃Sn wire the plan was to measure the tensile strain at which the I_c reaches its maximum with a parallel magnetic field of different magnitudes; this strain is taken as $\varepsilon = 0$. After this, a torsion measurement would be done, at 12 T and the $\varepsilon = 0$ found in the preceding measurement. For this purpose the insert was changed for wire-testing; when this modified insert was tested, it was found that the wire fixture was misaligned resulting in a large Lorentz force on the sample. Also, the copper tubes providing the current caused too high helium evaporation. Modifications to this setup are being performed for further testing at high magnetic field.

Table of Contents

Acknowledgements	i
Summary	ii
Chapter 1: Introduction	1
Chapter 2: Theoretical	2
2.1 Electrical properties	2
2.2 Mechanical properties.....	4
2.3 Bi-2223 tape superconductor	6
2.4 ReBCO CC tape superconductor.....	8
Chapter 3: Experimental	10
3.1 Bi-2223 and ReBCO tape measurement set-up	10
3.2 Nb ₃ Sn wire measurement set-up	13
Chapter 4: Results	15
4.1 COMSOL simulations	15
4.1.1 <i>Simple cylinder simulation</i>	15
4.1.2 <i>ReBCO tape simulation</i>	19
4.2 Bi-2223 tape measurements.....	26
4.3 ReBCO CC tape measurements	30
4.3.1 <i>Torsional strain test</i>	30
4.3.2 <i>Tensile strain test</i>	33
4.3.3 <i>Combined strain test #1</i>	35
4.3.4 <i>Combined strain test #2</i>	37
4.3.5 <i>Comparison of ReBCO measurements</i>	40
Chapter 5: Conclusion	42
References	44
Appendix: COMSOL settings	46

Chapter 1: Introduction

Multiple types of superconductors are now available for electromagnetic applications. In the present day, the workhorses in the field of superconductivity are niobium-tin (Nb_3Sn) and niobium-titanium (NbTi), which are cooled using liquid helium (at 4.2 K) [1, 2].

In the application of superconducting tapes/wires, they will be subjected to strain and stress, which affect the current carrying characteristics. When superconductors are used in coils to produce magnetic fields, as is the case for Nb_3Sn in the ITER fusion reactor, the electromagnetic Lorentz forces change the strain state and could lead to a reduced performance. The effect of a combination of strain and a magnetic field on the current carrying characteristics of Nb_3Sn is therefore of interest.

An advantage of using superconductors instead of normal conductors is that superconductors don't consume power, which allows for cheap operating costs; however, they have to be cooled in order to operate. Another advantage is the higher possible current density compared to normal conductors, which leads to higher magnetic field strengths and compact magnets. By avoiding Ohm's law, superconductivity can displace existing technology and enable new technology. For example, economic generation of electricity by nuclear fusion is not possible without superconducting magnets.

Looking towards the future, yttrium-barium-copper-oxide coated conductor (ReBCO CC) tapes in particular seem promising for applications, due to high current density, and the ability to operate them using liquid nitrogen (at 77 K) [3]. The future DEMO fusion reactor is one example in which ReBCO CC tapes might see large scale implementation, if made suited commercially and technologically for high field coils [4].

In the case of ReBCO CC tapes, research has been done concerning electro-mechanical properties including tensile, bending, compressive and torsional strain; magnetic field and temperature dependence [5-7].

Tensile and torsional strain dependence have already been investigated for this type of tape, also in the case of combined strains [8, 9]. In this assignment these experiments will be replicated with the purpose of validating the new probe. The new probe will be used for testing different ReBCO CC tapes from all available ReBCO manufacturers, aiming for the selection of the most suitable tape for the magnet coils in DEMO, the next nuclear fusion reactor after ITER.

This report will give an indication of how the effects of these combined strains on the critical current, I_c , have been measured and processed. Some measurements were done on a Bi-2223 tape to test the insert and instrumentation

Simulations in COMSOL, using the *finite element method* (FEM), have also been done to provide a better understanding on how the ReBCO CC tapes behave under mechanical loading, in particular under torsional strain, in the elastic stress-strain region. The model will be further refined in the future in order to understand better the possible differences between characteristics from various tape manufacturers using dissimilar layouts and materials.

Chapter 2: Theoretical

2.1 Electrical properties

In 1911 Kamerlingh Onnes (1913 Nobel Prize) discovered that the resistivity of mercury became zero at a temperature of 4.2 K, as indicated in Figure 1 [10]. This phenomenon is called superconductivity.

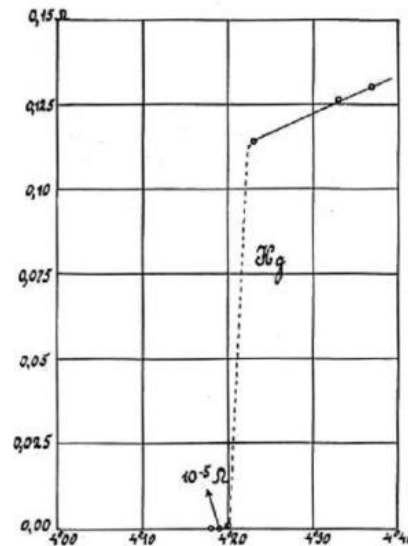


Figure 1: Discovery of superconductivity [10].

Mercury is one of the so called *Low Temperature Superconductors* (LTS), which need liquid helium in order to achieve their superconducting state. LTS-examples of well developed technical superconductors are niobium-tin (Nb_3Sn) and niobium-titanium (NbTi), which are used in MRI scanners, LHC magnets at CERN (NbTi) and ITER magnets at Cadarache (Nb_3Sn) [1, 2].

The discovery of the first of the *High Temperature Superconductors* (HTS) in 1986 by Müller and Bednorz (1987 Nobel Prize) made new applications feasible, as these conductors can operate at 77 K using the relatively cheap liquid nitrogen [11]. These HTS are often fabricated in tapes, and can be subdivided in two groups, based on the state of development:

- *First-Generation Superconductors* (1G HTS)
An example of these is the bismuth-based bismuth-strontium-calcium-copper-oxide ($\text{Bi}_2\text{Sr}_2\text{Ca}_2\text{Cu}_3\text{O}_{10}$ or *Bi-2223*).
- *Second-Generation Superconductors* (2G HTS)
These superconductors are based on rare-earth metals and barium-copper-oxide ((*RE*)*BCO*). Yttrium-barium-copper-oxide ($\text{YBa}_2\text{Cu}_3\text{O}_7$ or *YBCO*) is a 2G HTS example.

One can get an idea of the progress towards higher critical temperature superconductors by looking at Figure 2.

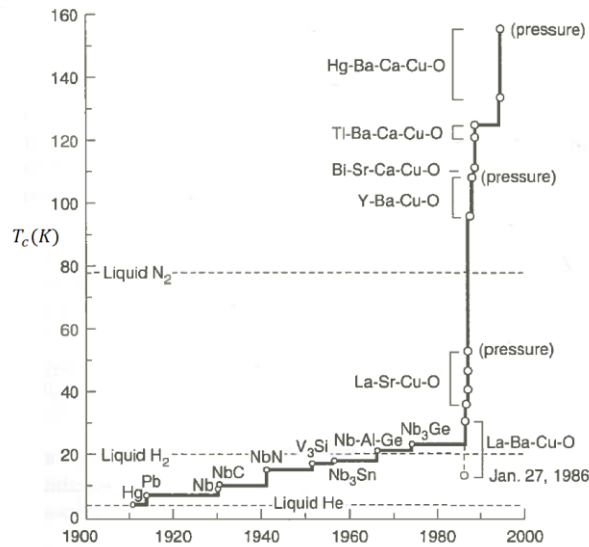


Figure 2: Superconducting critical temperature versus year of discovery [12].

The *electric field criterion*, E_c , is the magnitude (often 10^{-5} V/m is chosen) of the electric field above which a superconductor is no longer considered to be in its superconducting state. The threshold current at which this occurs is called the *critical current*, I_c . These definitions enable the characterization of the transition region by two simple quantities.

The *n-index* gives an indication of how the magnitude of the electric field depends on the current in the transition region; it is obtained by fitting measured $I - V$ data to the following equation:

$$E = E_c \left(\frac{I}{I_c} \right)^n \quad (1)$$

An example of a $I - E$ plot is given in Figure 3, which shows the results from an $I - V$ measurement using five voltage taps. The range of data used to determine the *n-index* is usually between E_c and the electric field a decade higher. Spread in adjacent measurement points results from thermal noise in the potentiometer circuit which is less significant at higher currents.

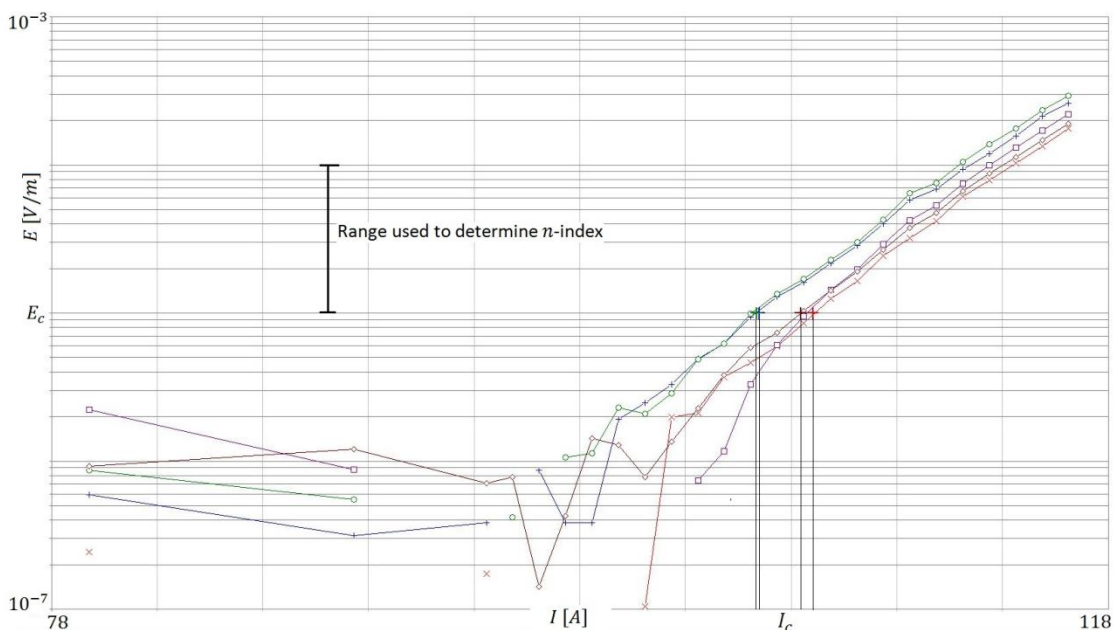


Figure 3: $I - E$ curve from ReBCO CC tape torsion measurement (150°) with 5 voltage taps and $E_c = 10^{-5} \text{ Vm}^{-1}$.

When mechanical load is applied to a superconductor, the current carrying characteristics can change. The current carrying capacity of a given superconductor is dependent on magnitude and direction of magnetic field, on temperature and on mechanical strain (ε): $E(I, \mathbf{B}, T, \varepsilon)$. These effects can be mapped by the I_c -dependence on those variables: $I_c(\mathbf{B}, T, \varepsilon)$. We will now look at some important mechanical properties which can have an effect on the critical current.

2.2 Mechanical properties

When a force is applied to a material, strain will be induced. The strain, ε , is defined by the formula

$$\varepsilon = \frac{\Delta L}{L_0} \quad (2)$$

Where L_0 is the rest-length of the sample at measurement temperature and ΔL the displacement caused by the load. If the force is applied in the longitudinal direction, the strain is considered to be *tensile* (ε_{tens}).

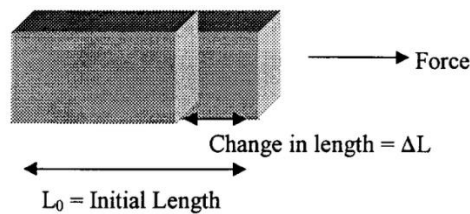


Figure 4: Material subjected to a force [13].

The stress, σ , experienced by a material is given by

$$\sigma = \frac{F}{A_0} \quad (3)$$

Where F is the applied force, and A_0 the cross-sectional area of the non-deformed sample.

Many mechanical properties of a material can be deduced from the so called *stress-strain curve* specific for that material. In this curve the relation between stress and tensile strain is plotted, as in Figure 5.

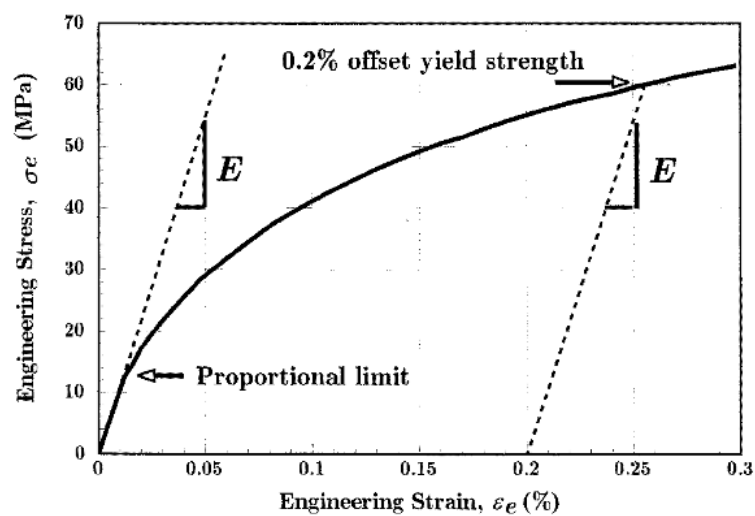


Figure 5: Stress-strain curve [14].

At low strains many materials approximately obey Hooke's law, which means that one can observe a linear relation between stress and strain in this region, up to the so called proportionality limit.

Young's Modulus is defined as the constant of proportionality in this region:

$$E = \frac{\text{stress}}{\text{strain}} = \frac{\sigma}{\varepsilon_{tens}} \quad (4)$$

The tensile strain can now be calculated in this region using the relation

$$\varepsilon_{tens} = \frac{F}{A_0 E} \quad (5)$$

After the proportionality limit has been reached, *strain hardening* will occur; the material will attempt to rearrange its internal structure. The amount of strain hardening depends on whether the material is ductile or brittle; brittle materials may break soon after reaching the proportionality limit.

In the lower part of the stress-strain curve, removing the strain will not leave a residual stress: the material behaves *elastically*. The elastic limit is around the proportionality limit, or slightly higher.

An important quantity in a stress-strain graph is the *yield stress*, σ_Y . This is the stress above which plastic deformation occurs in the material. Since it is not easy to distinguish the start of plastic deformation, σ_Y is often defined as the stress at which a permanent strain of 0.2% is induced.

Poisson's ratio, ν , is defined as the ratio between lateral and longitudinal strains experienced by a material. The lateral strains (which have the same value for an isotropic material) have the opposite sign of the longitudinal strain. For Poisson's ratio to be a positive number, it is defined as

$$\nu = - \frac{\varepsilon_{transverse}}{\varepsilon_{longitudinal}} \quad (6)$$

For metals the ratio is usually around 0.3 [15]. In the plastic regime ν increases to 0.5.

The *torsional strain*, experienced by a sample on which torsion is applied, is of complex nature and reaches a maximum in the midpoint of the width side of the tape's cross-section. This strain is defined by the formula:

$$\varepsilon_{tor} \equiv \frac{t\theta}{L} \quad (7)$$

Where t is the thickness of the sample and θ/L the twist pitch [9].

We define the strain at which I_c has degraded to 95% of the I_c measured in the virgin condition (I_{c0}) of the superconductor is called the critical tensile or torsional strain ($\varepsilon_{c,tens}$ and $\varepsilon_{c,tor}$ respectively).

After removing the strain, reversibility can be measured; the strain at which I_c recovers to 95% of I_{c0} is defined as the irreversible strain, $\varepsilon_{irr,tens}$ or $\varepsilon_{irr,tor}$ [5].

The need for mechanical strengthening is one of the reasons why a practical superconductor is made up from a combination of the superconducting material and other supporting layers. The production method used to make this superconducting tape or wire, as well as the need for thermal stability, place other requirements on the materials needed. The next section will look into the geometry of BSCCO- and ReBCO CC tapes.

2.3 Bi-2223 tape superconductor

The bismuth-strontium-calcium-copper-oxide (BSCCO) superconductor family consist of three members, with $\text{Bi}_2\text{Sr}_2\text{CaCu}_2\text{O}_8$ (Bi-2212) and $\text{Bi}_2\text{Sr}_2\text{Ca}_2\text{Cu}_3\text{O}_8$ (Bi-2223) being the superconductors of the three on which the majority of work is done.

The attractive quality of these conductors is the relatively high critical current at small magnetic fields. In high magnetic fields, the critical current density is higher than for Nb-based superconductors (both at 4.2 K) [16]. BSCCO is not very strong mechanically however.

BSCCO grains are grown on a silver substrate at high temperatures; silver has the property of being transparent to oxygen at high temperatures without reacting to it, making it a good substrate to grow the BSCCO on during the heat treatment process. A high critical current density is assumed to depend on parallel aligning of the BSCCO grains. This substrate material has drawbacks: silver is an expensive material, and not very strong. The silver can be strengthened to reach mechanic properties comparable to those of copper; because of this, silver-based alloys are sometimes used as matrix as well [17].

The BSCCO grains and the matrix are sheeted by silver or stainless steel layers. In case of a *quench*, which is the sudden, unexpected transition of a superconductor to the normal state, the sheets limit the maximum temperature by conducting the generated heat away from its source. The sheets also act as the main conducting part of the conductor when it is in normal mode, as the BSCCO grains have high resistivity when not in the superconducting mode [18]. The sheets also provide mechanical stability.

Width	2.98 mm
Thickness	0.231 mm
Young's Modulus [19]	77 GPa
Specified critical current	60 – 70 A
Critical temperature [16]	105 – 110 K

Table 1: Bi-2223 tape specifications.

The Bi-2223 tape used in the experiment was an old (~10 years) tape, and it was not clear whether the matrix consists of silver or of a silver based alloy, and whether the sheets consist of stainless steel or of silver.

Submerging a piece of the tape in hydrogen peroxide showed that the sheets were not made of silver; silver would have acted as a catalyst in the decomposition reaction of the hydrogen peroxide [20]. Samples were prepared in order to make images of the cross-sections of the Bi-2223 (and ReBCO) tapes. The optical microscope gave clear images of the Bi-2223 tape, as shown in Figure 6.

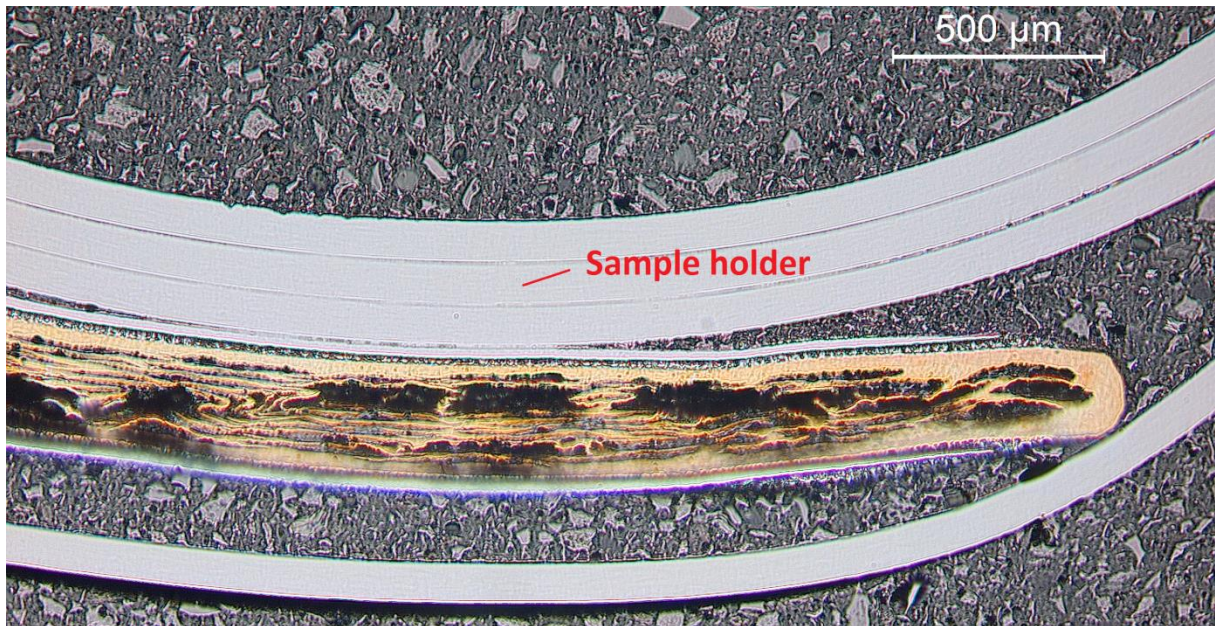


Figure 6: Optical image of Bi-2223 tape cross-section.

The thick bend lines seen in the picture consist of a holder used to align the tape during the sample preparation. A more zoomed in image, Figure 7, clearly shows the Bi-2223 filaments. It can also be seen that the steel sheath is not present on the edges of the tape.

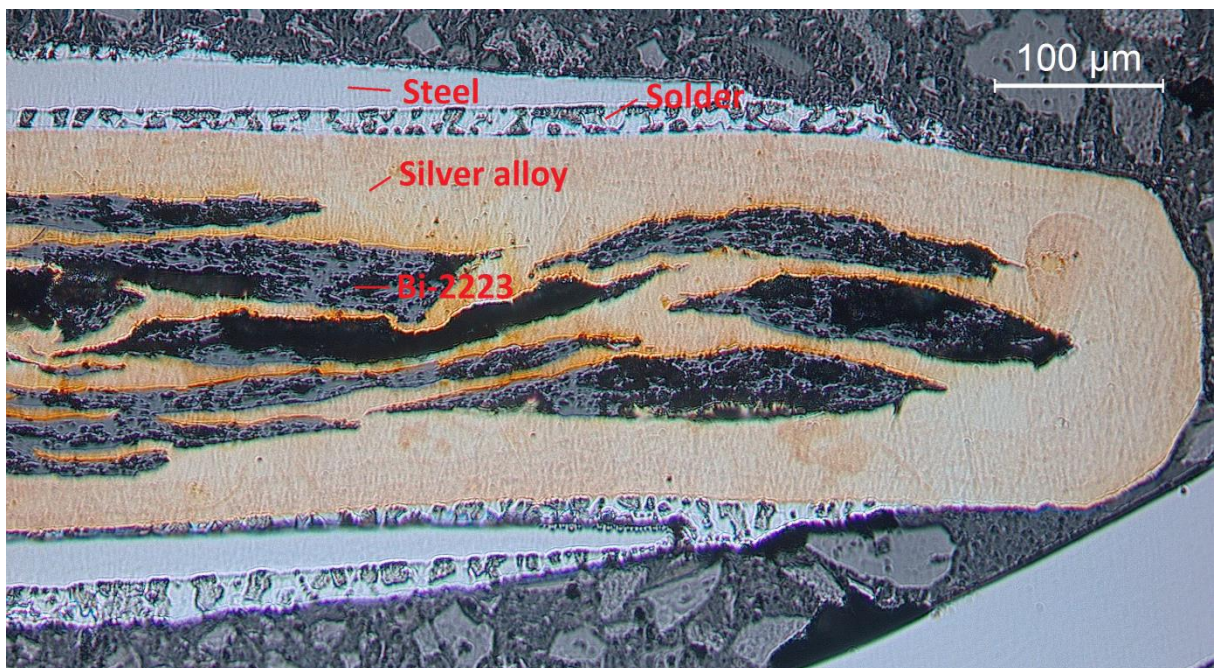


Figure 7: Optical image of Bi-2223 tape cross-section.

Besides its low mechanical strength, another disadvantage of a silver matrix is that its thermal expansion coefficient does not match that of BSCCO. By cooling a sample, compression will occur. If the different materials that make up a superconducting tape or cable have different expansion coefficients, stresses will develop during cooldown. In a BSCCO superconductor, the filaments have a large contact area with the surrounding matrix, and the difference in expansion rates is large ($\alpha_{AG} / \alpha_{BSCCO} \approx 1.5$) [21]. An externally applied tensile force will first have to compensate the strain caused by this compression effect before cracks can be initiated [22]. The compression effect itself can also cause cracks in the filaments; the effect is illustrated in Figure 8.

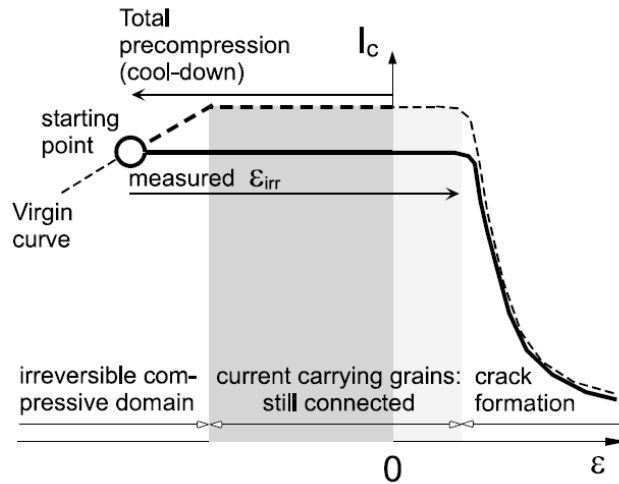


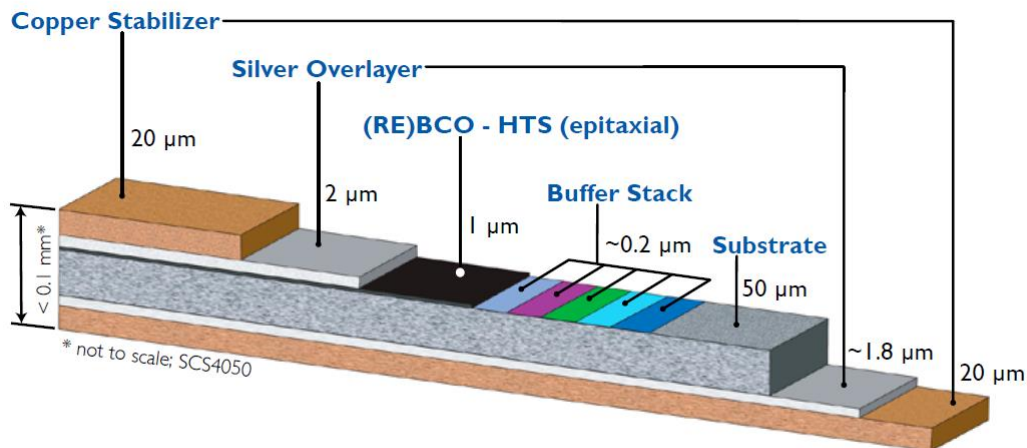
Figure 8: Effect of cooldown-compression on I_c [21].

2.4 ReBCO CC tape superconductor

The ReBCO samples used in the experiments are manufactured by SuperPower; the specifications of this SCS4050 tape are given in Table 2 and Figure 9.

Width	4.07 mm
Thickness	0.101 mm
Young's Modulus [23]	116.7 GPa
Specified critical current [24]	> 80 A

Table 2: SCS4050 tape specifications



Substrate Thickness:
50 μm Hastelloy® C-276 [or 100 μm for SF12100]
Substrate Yield Strength:
1200 MPa at 77 K

Substrate Resistivity:
125 $\mu\Omega\text{-cm}$ – higher resistivity leads to lower eddy current ac loss
Magnetic Properties:
non-magnetic, leads to lower ferromagnetic ac loss

Figure 9: SCS4050 specifications according to [25].

Grains in the ReBCO film have to align in order to allow current to be transported. To force this alignment, ReBCO CC tapes are fabricated by growing a ReBCO film on a Hastelloy substrate with the desired aligned texture.

Hastelloy is a nickel-molybdenum-chromium wrought face-centered cubic alloy, capable of withstanding high temperatures and high stress [26]. It provides both mechanical strength to the tape, as well as a base on which other layers can be grown. The Hastelloy layer is polished to a surface roughness of less than 2 nm after which ion beam assisted deposition (*IBAD*) of a magnesium oxide (MgO) based buffer stack takes place. A lithium manganese oxide (LMO) layer is also present in this buffer stack. The MgO-layer acts as a diffusion barrier, and as a base to grow the ReBCO layer on. Metal organic chemical vapor deposition (*MOCVD*) is used to grow the ReBCO film. This geometry of an ReBCO film on a metal substrate with metal-oxide buffer layers is called a *coated conductor* (CC) [11].

A silver layer is put on top of the ReBCO film to provide good electrical contact. A copper layer that surrounds the entire tape provides mechanical and thermal stabilization. These silver and copper layers are the main conducting materials in the tape when the ReBCO film is no longer in its superconducting state [27].

The compression effect discussed for the Bi-2223 tape is not very significant in the ReBCO CC tape as the relative contact area between the ReBCO and the surrounding material is much smaller.

The properties of the materials at 77 K of which the SCS4050 tape consists are presented in Table 3; the buffer layers are omitted from this table.

Material	Poisson's ratio	Young's Modulus [GPa]	Density [kgm^{-3}]	Yield stress [MPa]
Copper	0.34 [28]	136 [28]	8940 [29]	38.5 [30]
Hastelloy C276	0.307 [31]	216 [32]	8890 [33]	440-470 [32]
ReBCO	0.3 [34]	157 [35]	6300 [36]	684-748 [32]
Silver	0.364 [37]	89.8 [37]	10630 [37]	45-76 [37]

Table 3: Material properties at 77 K .

Figure 10 shows the ReBCO layer cross-section. The ReBCO layer and functional layers measure a height of $3\text{ }\mu\text{m}$ instead of the $1.4\text{ }\mu\text{m}$ given by the specifications [24, 25]. This could be an effect of smearing during the polishing of the sample.

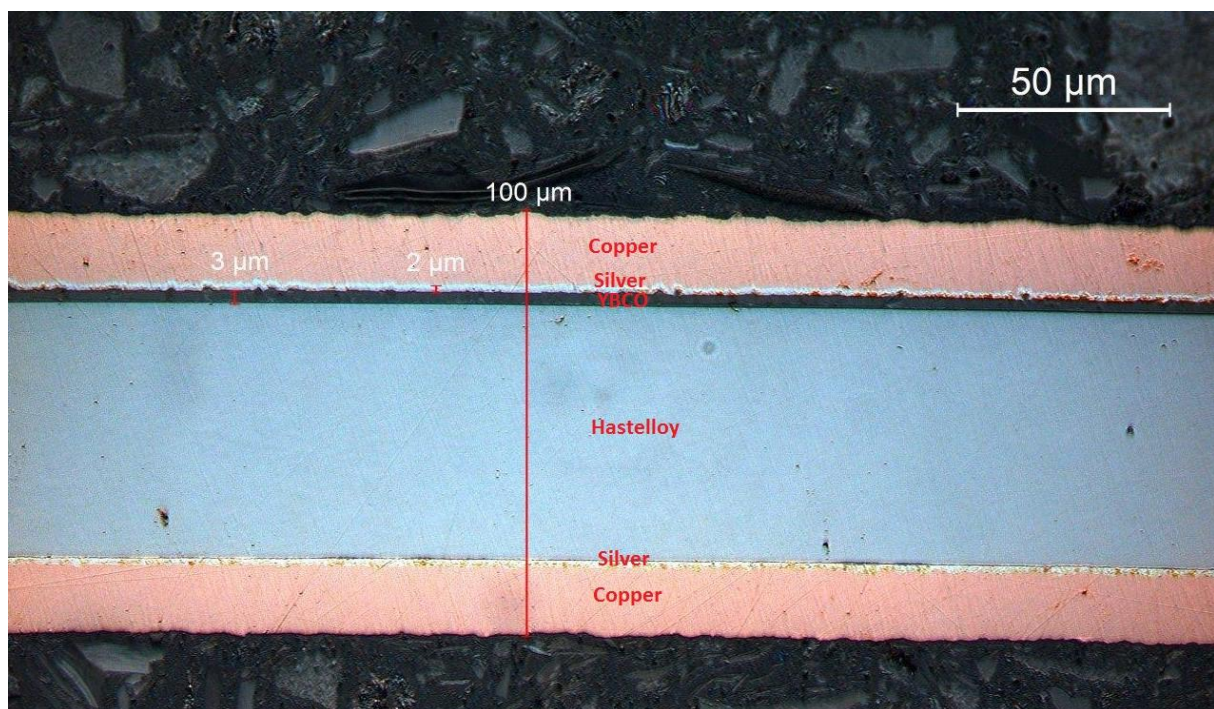


Figure 10: Optical image of ReBCO tape cross-section.

Chapter 3: Experimental

3.1 Bi-2223 and ReBCO tape measurement set-up

For the measurements, an insert was needed that would allow torsional and tensile strains to be applied to the sample, while cooled down from room temperature (RT) to 77 K by insertion in a cryostat filled with liquid nitrogen. This insert is presented in Figure 11.

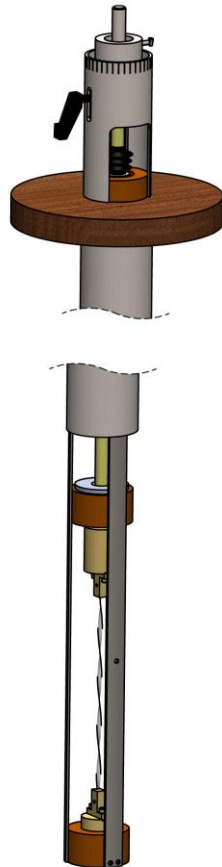


Figure 11: Insert design.



Figure 12: Motor stage.

The motor stage shown in Figure 12 is located above the insert and allows the sample to be stretched in very small increments.

While knowing the magnitude of the displacement is enough to calculate the tensile strain, there is the problem that not only the sample but also the insert stretches: therefore knowing the displacement one controls by the motor stage is of no use. An extensometer could provide the correct displacement, but would not work well when torsion is applied. Therefore a 150 N load-cell is used to determine the tensile load on the sample resulting from the displacement.

This load-cell uses a piezoelectric material to determine the applied load: for every 1 N increase of the load, the load-cells output increases by 13.6 μV . Knowing the applied load, one can calculate the applied tensile strain defined by eq. (5).

Torsion can be applied by rotating the cylinder to which the sample is mounted at the top. This can be done by pushing a small extension that is also used to indicate the applied angle.

To help with determining this angle, markings have been applied at 10° intervals on the insert, as can be seen in Figure 13.

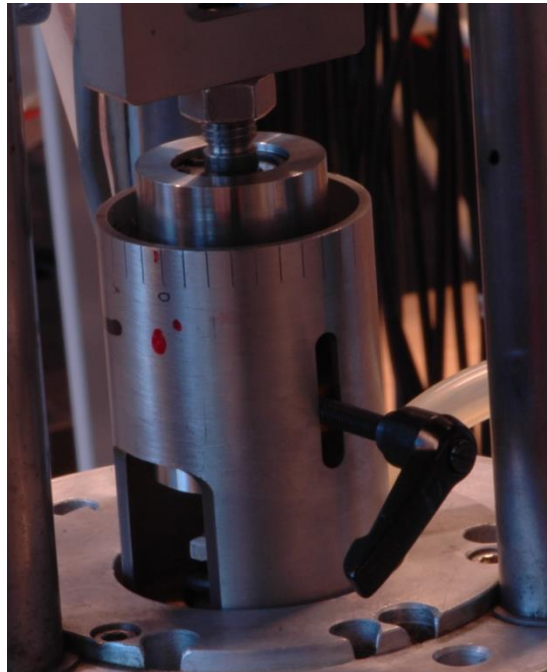


Figure 13: Top part of the insert.

In this figure one can also see the handle used to fix the angle, once it is applied. This handle can move freely in the vertical direction to allow tensile strain to be applied.

The sample is soldered to copper blocks which also act as current leads. A copper cable is used to enable current to be provided while the sample rotates, as can be seen in Figure 14. The length of the sample between the blocks is 17 cm .

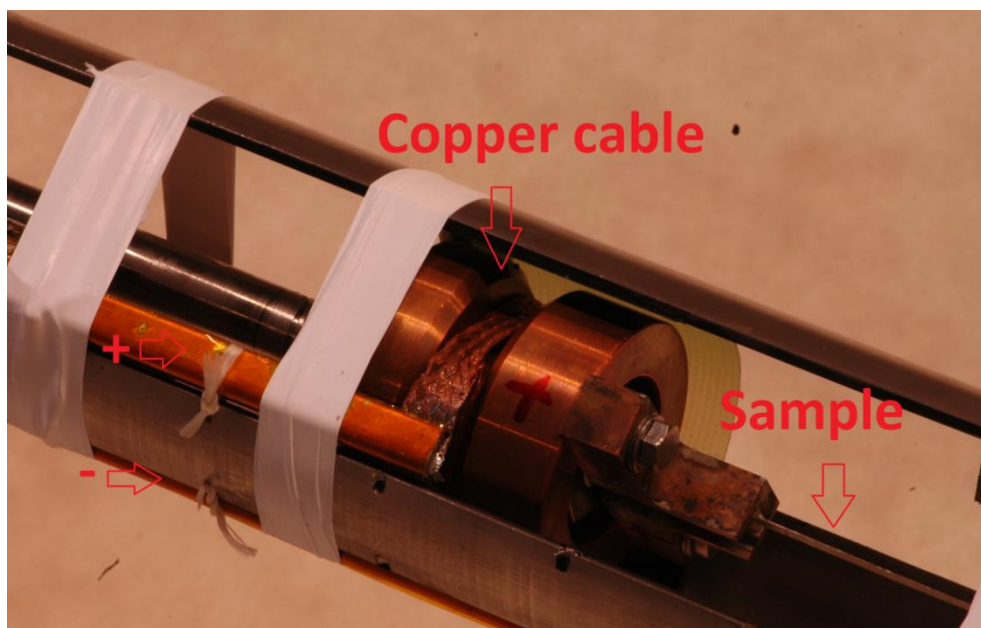


Figure 14: Top current lead.

For $V - I$ measurements the so called *four-probe method* is used, in order to improve accuracy over the more traditional two-terminal method. This accuracy (nV range) is needed because of the small resistance levels involved. In the four-probe method, each current lead and each voltage lead is a distinct electrical contact without overlap. As a result, the contact resistance of the voltage tap will become part of the lead, and as the impedance of the potentiometer-input is very high, no current will flow in that circuit. Therefore only the potential difference between the voltage contacts can be measured.

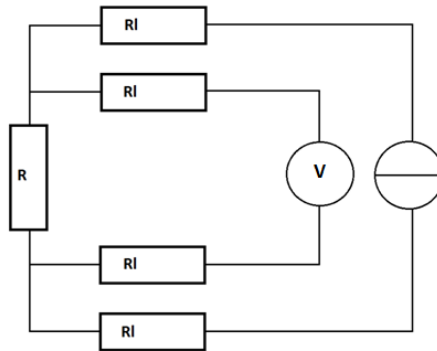


Figure 15: Four probe method schematic.

To investigate homogeneous electro-mechanical properties across the length of a sample, multiple voltage taps can be used; in this experiment five voltage taps, soldered to the sample, are connected to a terminal, as can be seen in Figure 16; from this terminal wires run to potentiometers. These voltage taps have 15 mm spacing and are located in the middle of the sample in order to avoid boundary effects from the soldered sample ends.

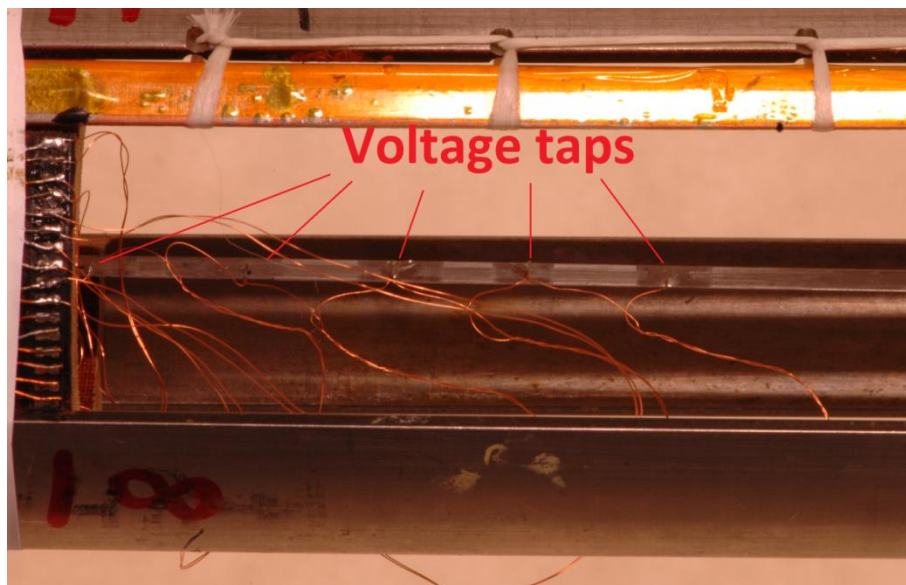


Figure 16: Voltage taps, 15 mm spacing.

3.2 Nb₃Sn wire measurement set-up

For the Nb₃Sn wire the idea was to measure I_c at varying tensile strain, with a parallel magnetic field of different magnitudes, $I_c(B_{||}, T = 4.2 K, \varepsilon_{tens}, \varepsilon_{tor} = 0)$. Because of the thermal mismatch, discussed earlier for the Bi-2223 tape, a maximum I_c is expected at small applied strain; this strain is taken as $\varepsilon_{tens} = 0$, and as such the wire can be defined to have a negative strain at the start of the measurements. The Nb₃Sn wire would need to be cooled using liquid helium (4.2 K).

After this, a torsion measurement would be done on a new sample, measuring I_c as a function of ε_{tor} , at 12 T and the $\varepsilon_{tens} = 0$ found in the preceding measurement, $I_c(B_{||} = 12 T, T = 4.2 K, \varepsilon_{tens} = 0, \varepsilon_{tor})$.

One problem that comes into play when measuring at high magnetic fields is the Lorentz force on by the sample; because the magnetic field is not uniform over the sample length, the sample will see a transverse magnetic field contribution. The field strength isoclines are depicted in Figure 17.

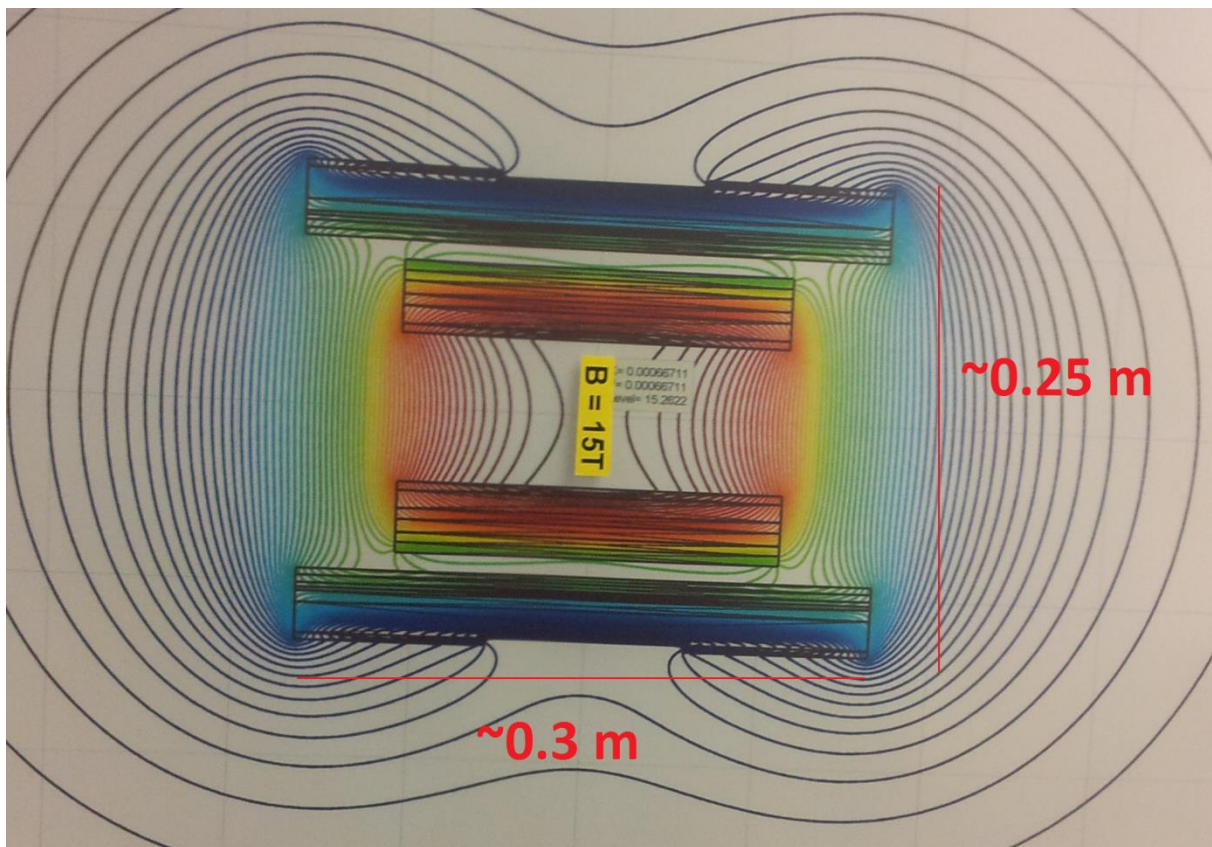


Figure 17: Magnetic field isoclines.

This Lorentz force makes it important to center the sample as much as possible. A reduction of sample length also helps in reducing the Lorentz force as it will decrease the bending caused by the Lorentz force itself. Bending will increase the parallel magnetic field component on the wire, in turn increasing the Lorentz force.

To reduce this positive feedback, the sample length was reduced to 11 cm for the Nb₃Sn wire. A small metal cylinder made it possible to detect sample deflection from the centerline by measuring the resistance between the cylinder and the sample.

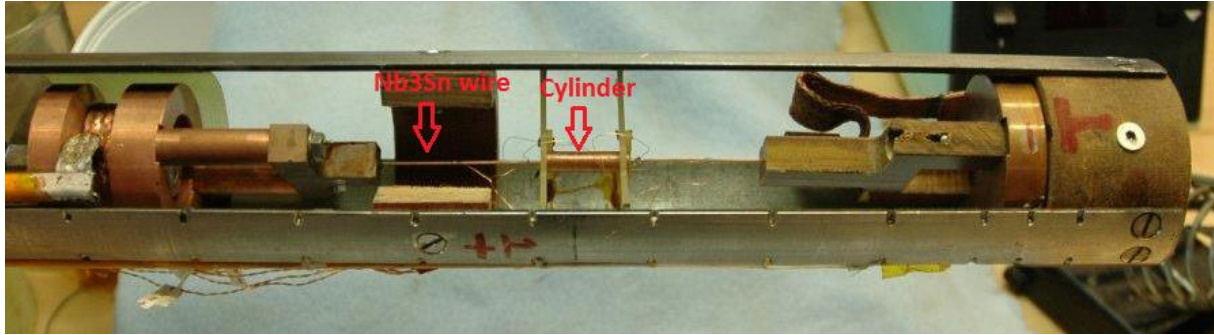


Figure 18: Insert modified for wire testing.

When this modified insert (Figure 18) was tested, it was found that the Lorentz force on the sample was too large, as the sample touched the cylinder. Also, the copper tubes providing the current caused too high helium evaporation due to the press connection and the flexible coupling between the upper lead allowing for the rotation. Ideas for improvement are cooling of the copper tube lead with a flow of helium gas or replacement of the rotating spiral made from copper Litz wire by superconducting material. Proper alignment with the applied magnet field and supporting of the sample would also be needed to conduct this experiment.

Chapter 4: Results

4.1 COMSOL simulations

To get a better understanding of how the ReBCO tape behaves under torsional strain, simulations were done in COMSOL using the *finite element method* (FEM). The FEM is a numerical technique that finds approximate solutions to boundary value problems by minimization of an error function [38]. FEM uses small subdomains (called finite elements) and simple equations to approximate a larger domain obeying more complex equations. The entire collection of the finite elements in the geometry is called the *mesh*; an example of this is shown in Figure 19. The mechanical module requires the Young's Modulus, Poisson's ratio and density of the materials involved. FEM assumes isotropic mechanical properties and can only operate in the elastic stress-strain regime.

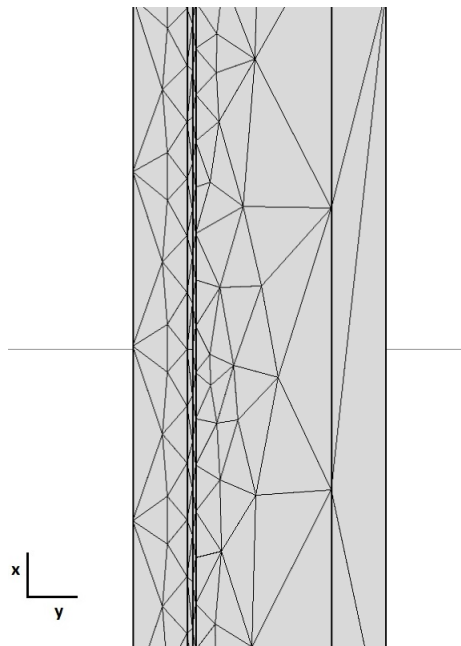


Figure 19: FEM mesh example.

4.1.1 Simple cylinder simulation

To apply torsion in COMSOL, one has to define a cylindrical coordinate system and apply a force in the θ -direction. To make sure that the torsion worked well, a simple cylinder, made out of just one material, was simulated first.

There are two possible ways to apply a force in the θ -direction on the cylinder:

- One can give one end a fixed constraint and apply a boundary load on the other; this gives some boundary effects on the fixed end.
- The other method is to apply a boundary load on one end and an opposite load on the other.

It was found that the last method did not always provide a stationary solution. Using a long enough sample length should allow the boundary effect present in the first method to be only a local influence. Therefore the first method is used. Its validity will now be shown by comparison with analytical results.

The longitudinal direction of the sample was chosen to be in the z -direction in both the Cartesian and cylindrical coordinate systems, so that its cross section coincides with the xy -plane. The r -coordinate

in the cylindrical system was defined in a way to place its origin in the middle of the cross section, as can be seen in Figure 20-21.

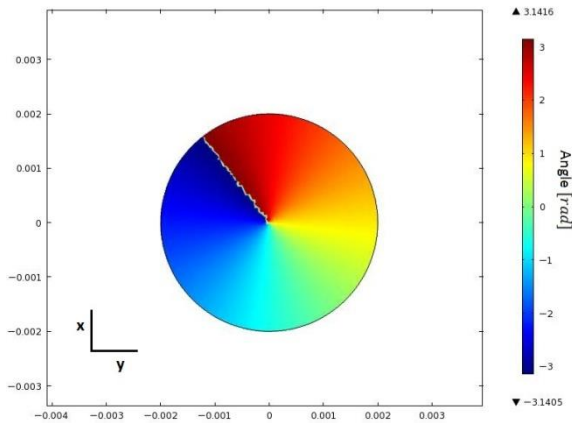


Figure 20: θ -coordinate across cross-section.

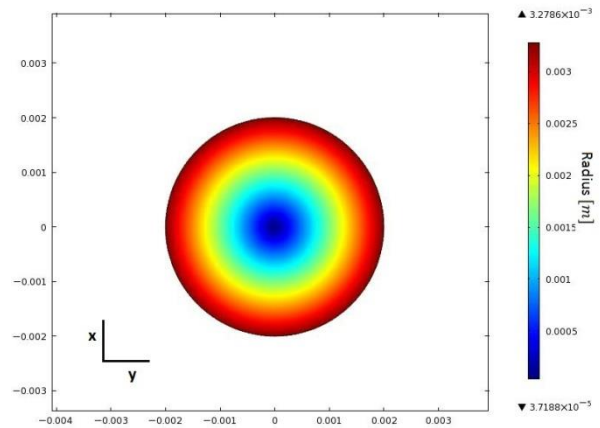


Figure 21: r -coordinate across cross-section.

From these 2D-plots, it seems like the cylindrical coordinate system works fine; a 3D-plot however shows a z -dependence of both the r - and θ -coordinates, as can be seen below.

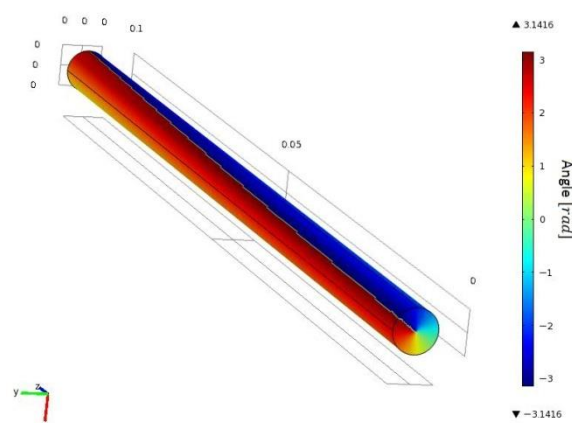


Figure 22: θ -coordinate across cylinder.

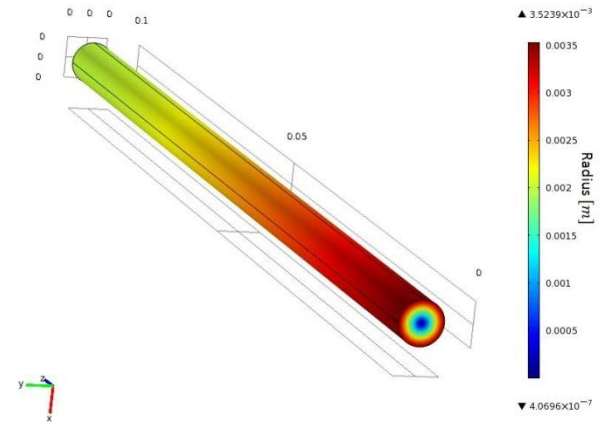


Figure 23: r -coordinate across cylinder.

This is probably the reason that the deformed geometry shows some volume changes as well as torsional deformation.



Figure 24: Deformed cylinder.

To see how this peculiarity causes problems, we first look at 1D-plots with data from the centerline of the cylinder ($r = 0, 0 \leq z \leq L$), indicated below in red.

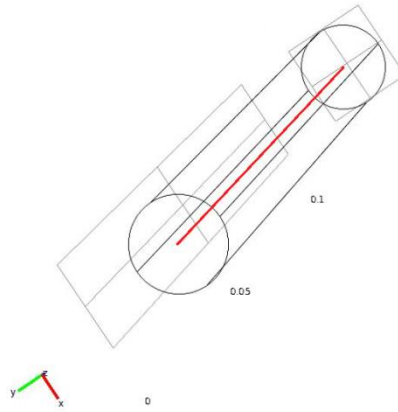


Figure 25: Red centerline.

Figure 26 shows the displacement along this line, where the fixed end ($z = L$) is defined to have zero displacement.

While a linear relation between z and the displacement is expected along this centerline, one can not only see some small (expected) boundary effects at the fixed end, but also very large displacements at the end where the boundary load is applied.

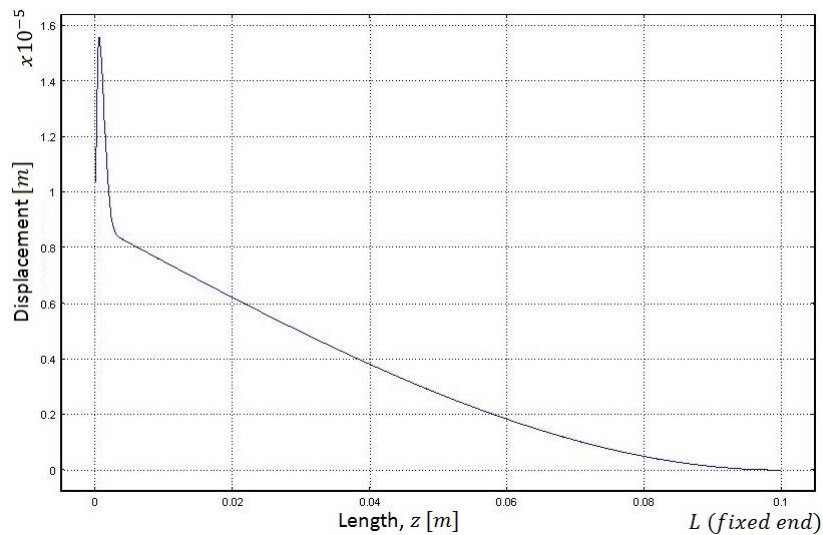


Figure 26: Displacement along centerline.

The stress in the sample also shows very large boundary behaviour (Figure 27). The stress used in this figure is the *von Mises stress*, which is used to predict yielding of materials under multi-axial loading conditions [39].

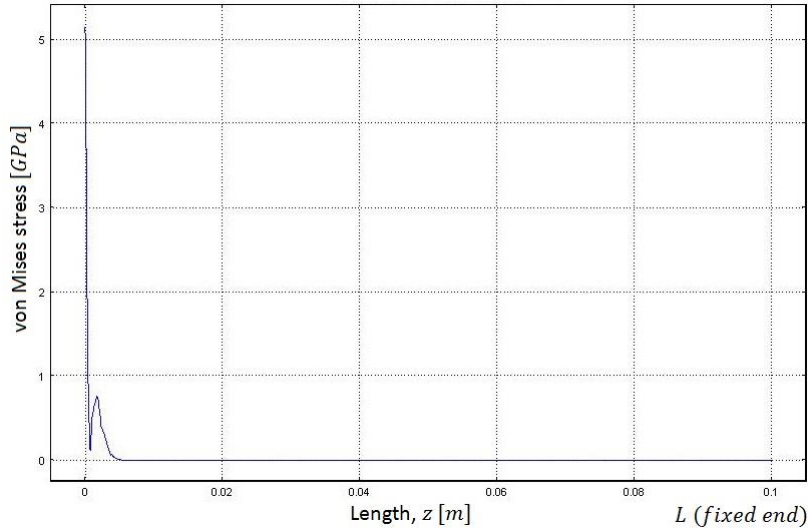


Figure 27: Stress along centerline.

To see if the region in which the displacement varies linearly gives valid torsional deformation, a comparison is done with the analytical formula. For these plots the line indicated below, showing behaviour along the radial direction at $z = L/2$, is used.

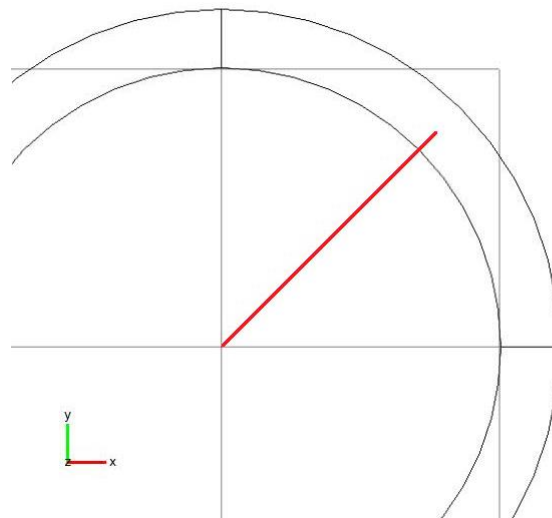


Figure 28: Radial component, r (red line).

For a cylinder of radius R subjected to a torque T , the maximum shear stress, τ_{max} , has the magnitude [40]

$$\tau_{max} = \frac{2\vec{T}}{\pi R^3} \quad (7)$$

$$\vec{T} = \langle \vec{r} \rangle \times \vec{F} \quad (8)$$

$$|T| = \frac{R|F|}{\sqrt{2}} \quad (9)$$

$$|\tau_{max}| = \frac{\sqrt{2}|F|}{\pi R^2} \quad (10)$$

For the force and radius used in the simulation, the analytical formula gives $\tau_{max} = 2.25 \text{ GPa}$, while the maximum shear stress in the simulation has a magnitude of 2.09 GPa , shown in Figure 29 where shear stress versus the radius is plotted, a difference of around 8%. From this it is concluded that the

method of applying torsion can accurately be used as long as one avoids the boundary regions where the force is applied.

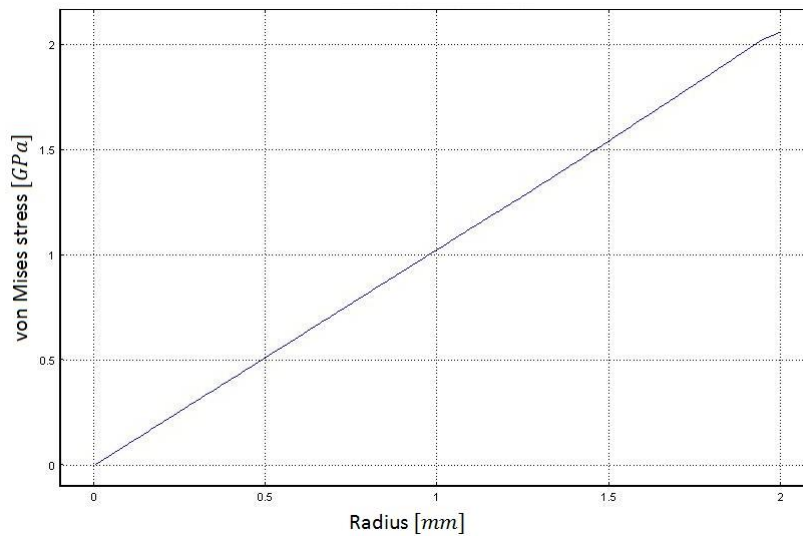


Figure 29: Stress along r -coordinate

4.1.2 ReBCO tape simulation

The geometry of the ReBCO tape is not well suited for simulation: because of the large aspect ratio length:width:thickness, the mesh needed for FEM consists of a very large number of elements. Three approximations were done to make the mesh manageable for computing:

- The width of the tape was reduced from 4.07 mm to 0.7 mm, and the length from 17 cm to 1 cm.
- The mesh density in the longitudinal direction of the tape was decreased compared to the density in the other two directions.
- Thin functional layers of MgO and LMO were omitted from the used geometry, as well as the thinnest silver layer. In the case of the MgO, the stress-strain profiles depend strongly on the crystal orientation [41]. It would be necessary to know the used crystal orientation in the buffer stack if one wanted to include this layer.

So the simulations were done using a model of the tape, consisting of 5 layers, with reduced width and length compared to the real ReBCO tape. The used parameters are visible in Table 4.

Actual geometry [25]		Simulation geometry	
Material	Thickness (μm)	Material	Thickness (μm)
Copper	20	Copper	20
Silver	2	Silver	2
ReBCO	1.2	ReBCO	1.27
LMO	0.030		
MgO	0.040		
Hastelloy	50	Hastelloy	50
Silver	1.8		
Copper	20	Copper	21.8

Table 4: SCS4050 Tape and simulated tape geometries.

A reduction of boundary effects was achieved by constructing steel cylinders at the ends of the tape, and applying the load on these. This used geometry is shown in Figure 30. In the following part one

should look at the qualitative results as the different geometry ratios used in the simulations compared to the experiment do not allow direct quantitative comparisons.

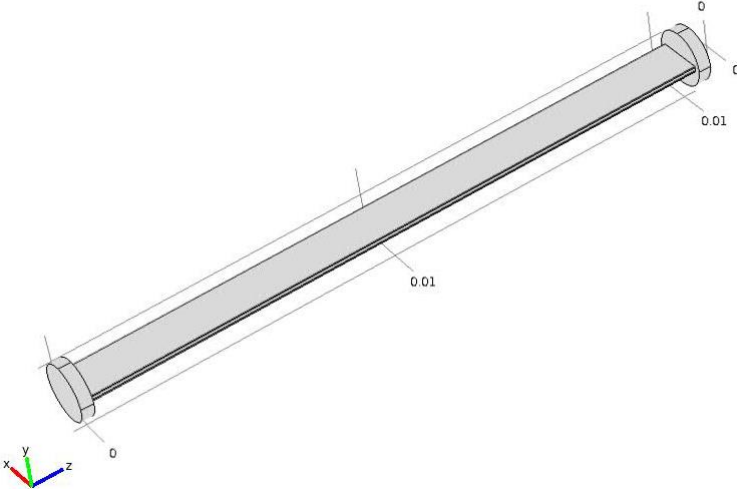


Figure 30: Simulated shape consisting of 5 layers, 1 cm length.

Analog to the cylinder simulation, data from a line between $z = 0$ and $z = L$, situated in the middle of the ReBCO layers cross-section, is used as shown below.

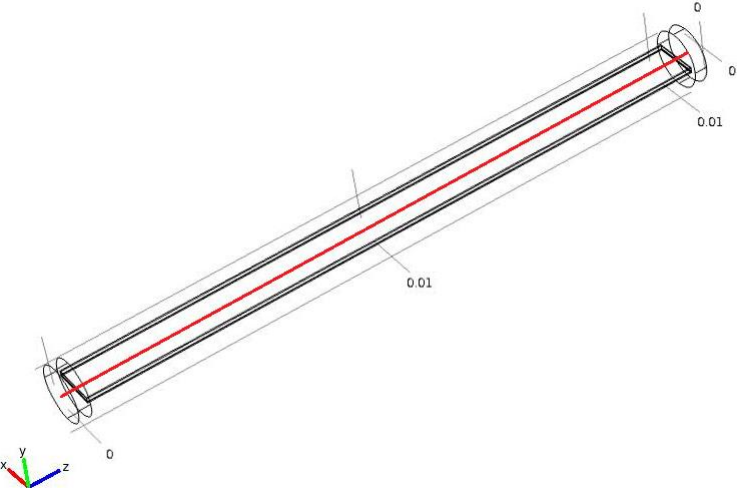


Figure 31: Red centerline.

The simulation boundary effect in the displacement seems to be reduced by using these cylinders (Figure 32).

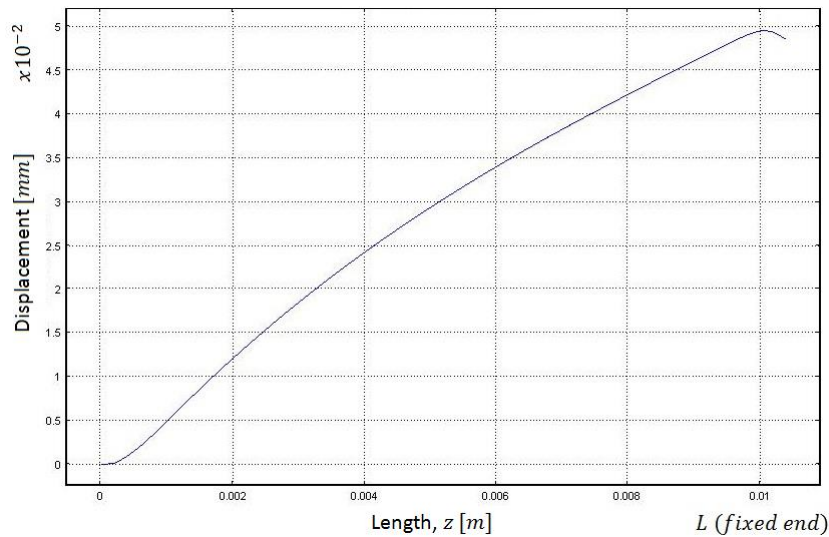


Figure 32: Displacement along z-direction at ReBCO layer height for $L = 1$ cm.

If one looks at the stress along this line though, a large boundary effect can again be seen.

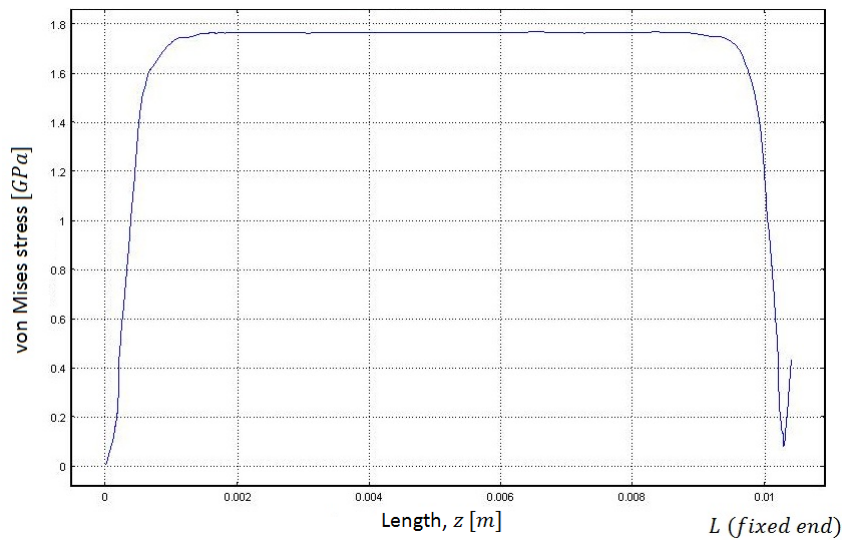


Figure 33: Stress along z-direction at ReBCO layer height for $L = 1$ cm.

When the ends consisting of the steel cylinders are omitted from the results however, the stress along the longitudinal direction is found to be very uniform (Figure 34). This leads to the prediction that homogeneous results in the elastic region will be found along the midsection of the tape except for the very ends.

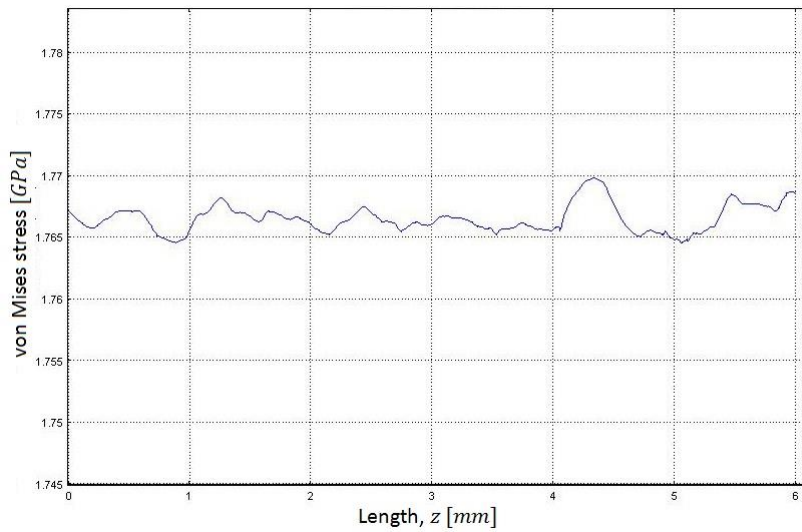


Figure 34: Stress along z -direction at ReBCO layer height for $L = 1$ cm. Note the small scale on the vertical axis.

So the boundary regions were found to make up only a small section of this 1 cm long piece of tape. As only a small homogeneous section is needed in the simulation, it was decided to reduce the sample length further to 4 mm, which made possible the use of a higher mesh density. This length still shows an adequate section of constant stress (Figure 35).

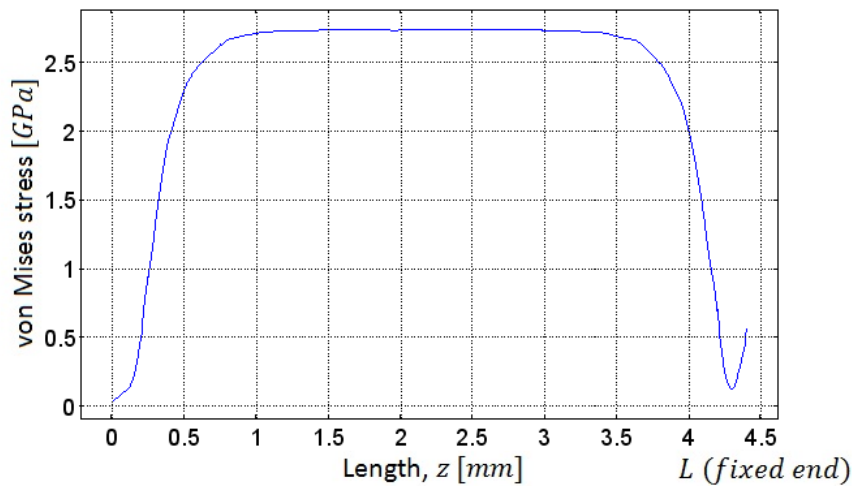


Figure 35: Stress along z -direction at ReBCO layer height for $L = 4$ mm.

The next section looks at the cross plane of the tape located at $z = L/2$. Figure 36 shows the stress-profile of this plane.

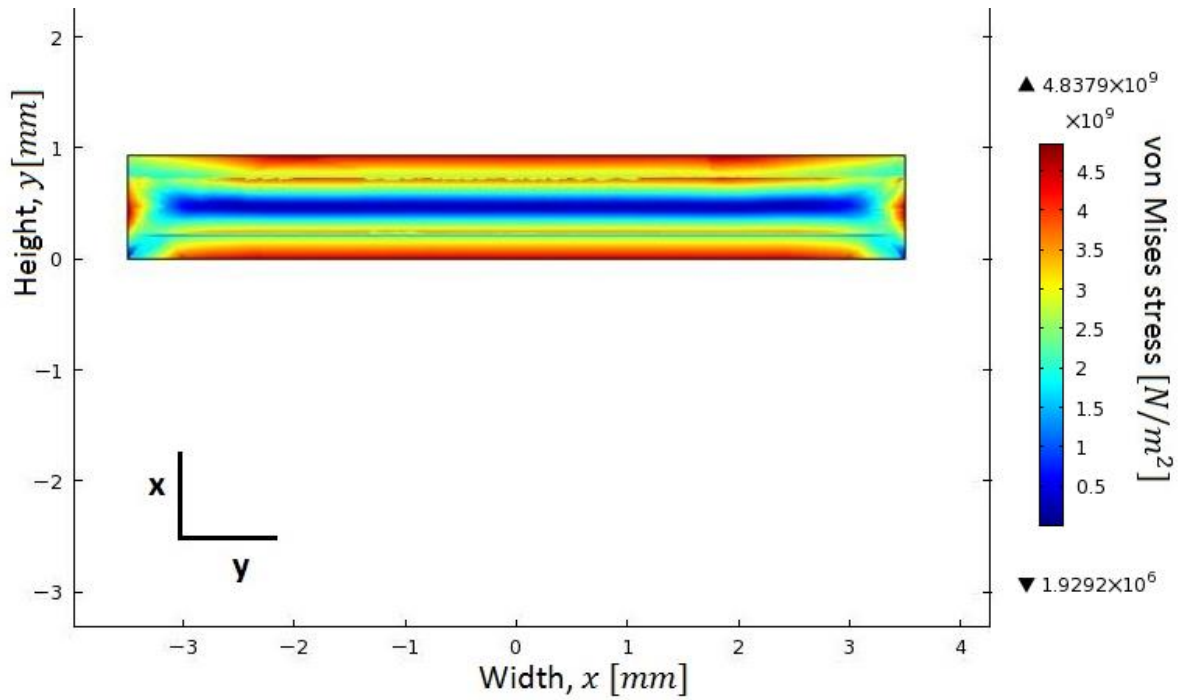


Figure 36: Stress profile of cross section.

To get a better understanding of this stress-profile, we again resort to 1-dimensional plots. First we look at the line along the width of the tape, at $z = L/2$ and at the middle of the ReBCO film.

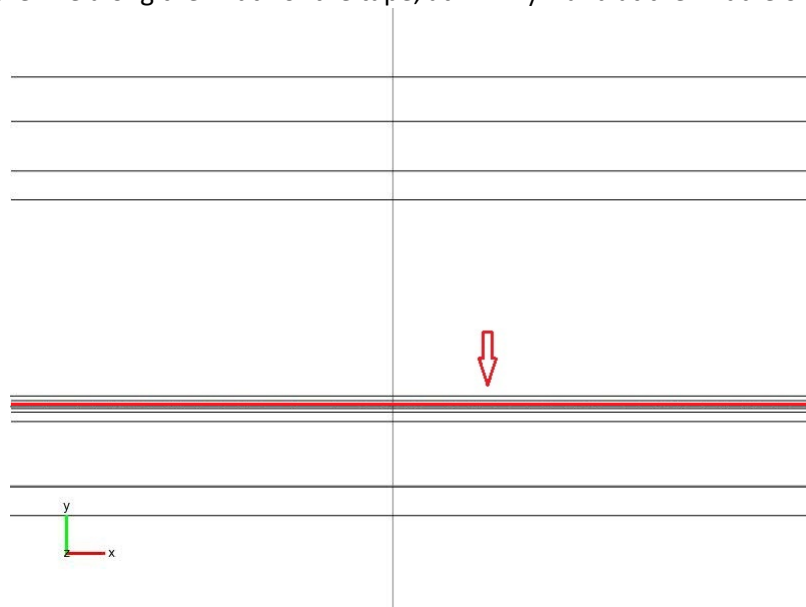


Figure 37: Data-line along sample width, at ReBCO layer height.

The stress along this line shows a constant stress region in the midsection of the tape, with a decrease at the ends of the width-section. The increasing stress at the very ends is thought to result from simulation-based boundary effects.

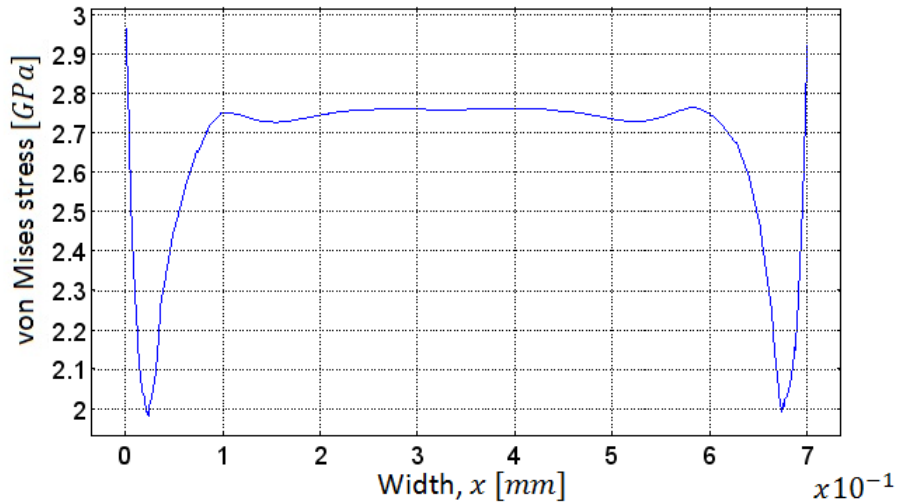


Figure 38: Stress along sample width, at ReBCO layer height.

Next we look at the data from the line across the height of the tape, at $z = L/2$ and at the middle of the width section, indicated in Figure 39.

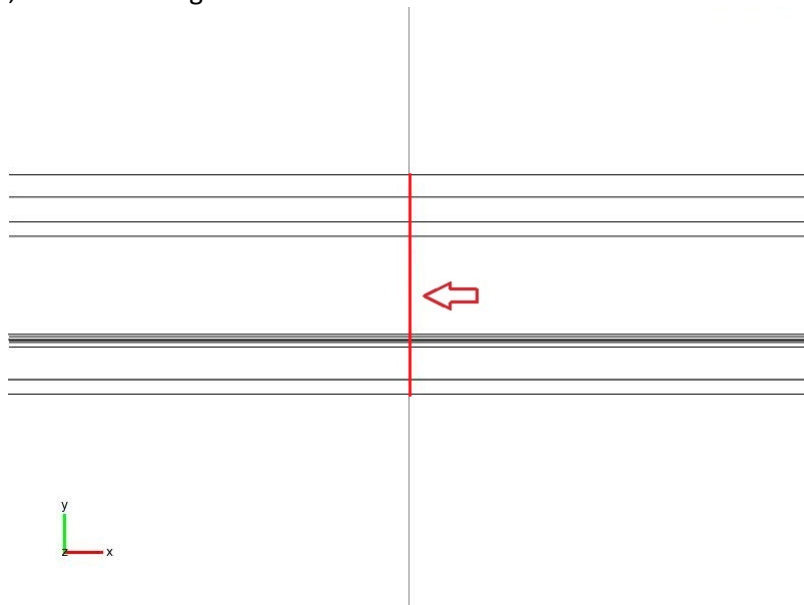


Figure 39: Data-line along sample height.

In Figure 40 we can see the distribution of stress along this line:

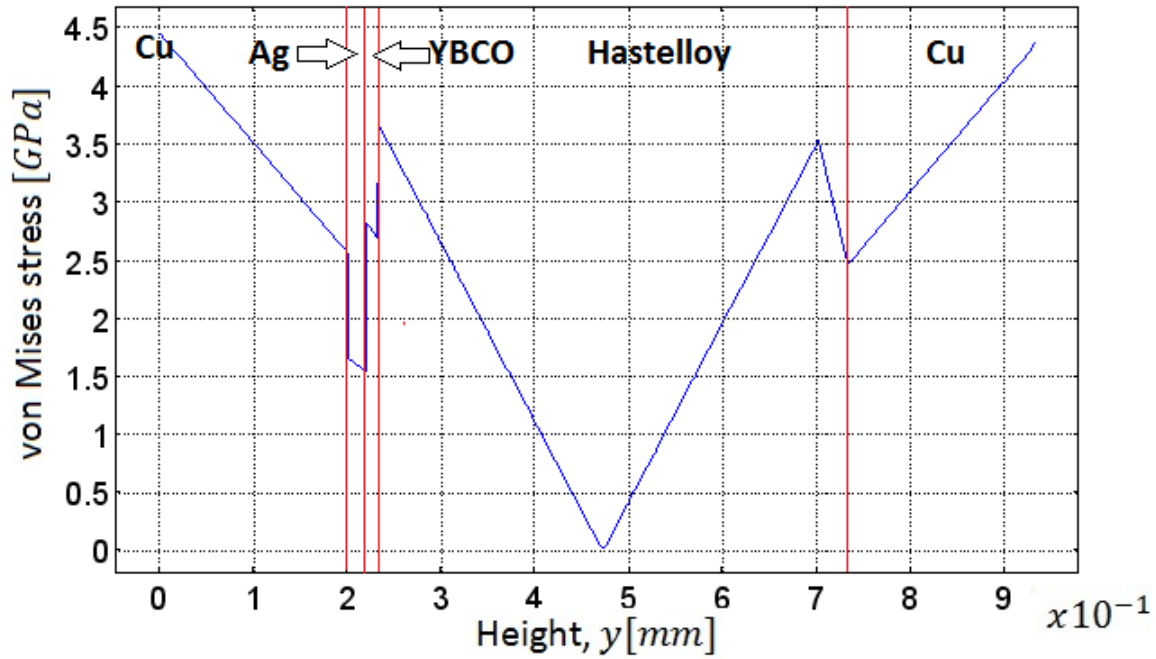


Figure 40: Stress along sample height.

We can get an idea of the effect of torsional strain on the I_c by comparing the ratio of the stresses found in Figure 40 to the ratio of the yield stresses of the respective materials (Table 5).

	Stress in Figure 40 [GPa]	Yield stress (77K) [MPa]	$\frac{Stress}{Yield\ stress}$	$\frac{Stress}{Yield\ stress} / \frac{Stress_{Cu}}{Yield\ stress_{Cu}}$
Copper	4.5	38.5 [30]	116.9	1
Silver	1.6	45-76 [37]	21.1-35.6	0.18-0.30
ReBCO	2.8	684-748 [32]	3.74-4.10	0.032-0.35
Hastelloy	3.7	440-470 [32]	7.87-8.41	0.067-0.072

Table 5: Yielding ratios found in the simulation.

From comparing the stress/yield stress ratios, it can be concluded that the copper layer is the first to show plastic deformation. When the copper starts to yield, redistribution of stress will take place. The silver layer is second to leave the elastic region.

4.2 Bi-2223 tape measurements

Measurements were done on a Bi-2223 tape with relevant specifications listed in Table 1. This experiment mainly served to see if the set up worked, using Bi-2223 instead of the more expensive ReBCO tape. The electric field criterion used for this tape is 10^{-4} Vm^{-1} . All measurements were done at self field.

For this Bi-2223 tape the critical current was measured at varying torsional strain ($\Delta\theta = 30^\circ$ or 60°), at fixed (zero) tensile load: $I_c(T = 77 \text{ K}, \varepsilon_{tens} = 0, \varepsilon_{tor})$. The tensile load was set to a minimum by operating the motor stage until the load cell showed an increase of its output voltage, meaning the sample was no longer slacked. Results are shown in Figure 41-43. The measurements done at applied torsion are shown in black, the reversibility measurements in white, for each of the five voltage taps.

Voltage tap 1 started to deviate from the other taps starting around $\varepsilon_{tor} \sim 0.2\%$, showing large I_c and n -value degradation. After inspecting the sample it was found that it had buckled at voltage tap 1, probably due to a too large amount of solder.

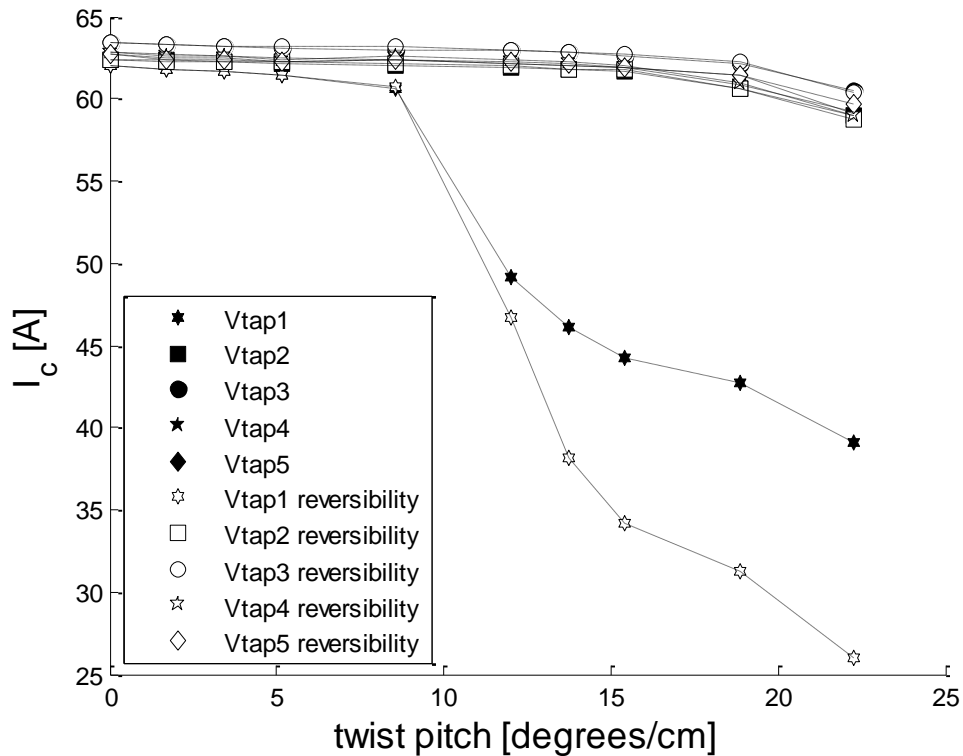


Figure 41: Behaviour of I_c for Bi-2223 tape during pure torsion test.

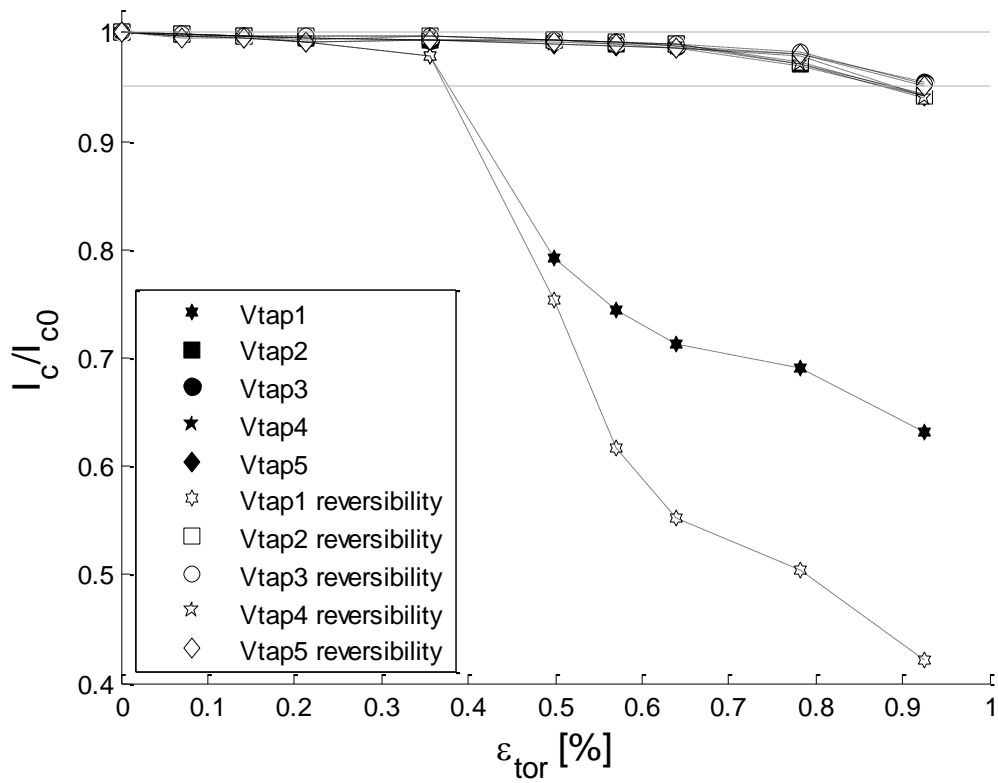


Figure 42: Behaviour of I_c/I_{c0} for Bi-2223 tape during pure torsion test.

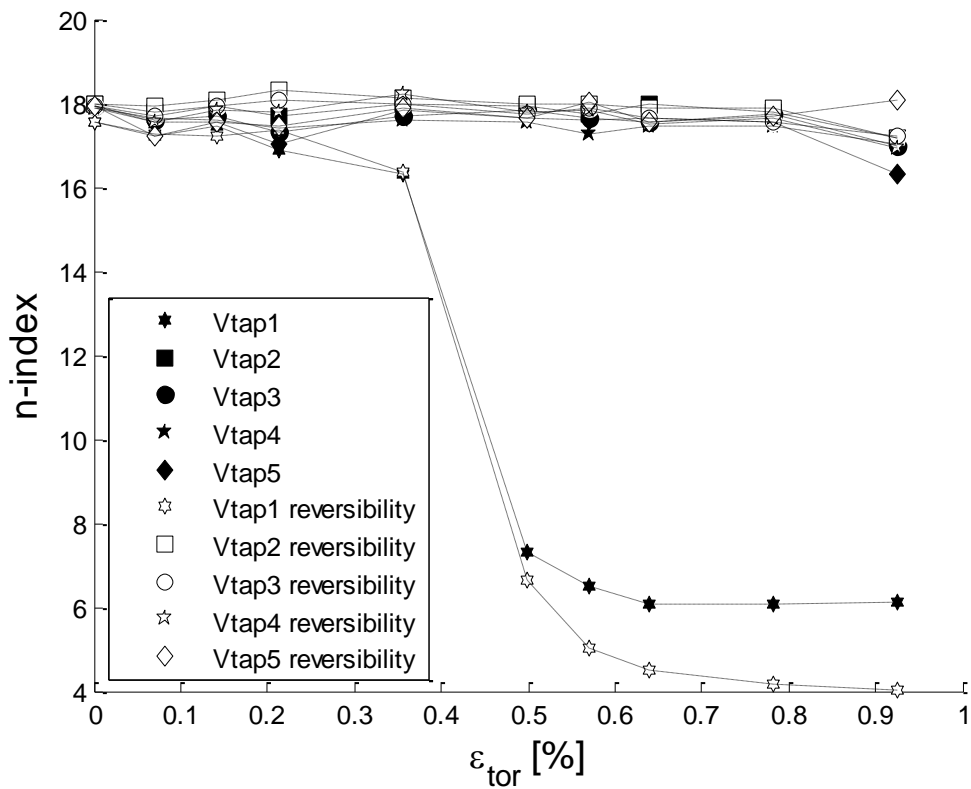


Figure 43: Behaviour of n -index for Bi-2223 tape during pure torsion test.

We will now look closer at the data from the other four taps, omitting voltage tap 1-data in Figure 44-46.

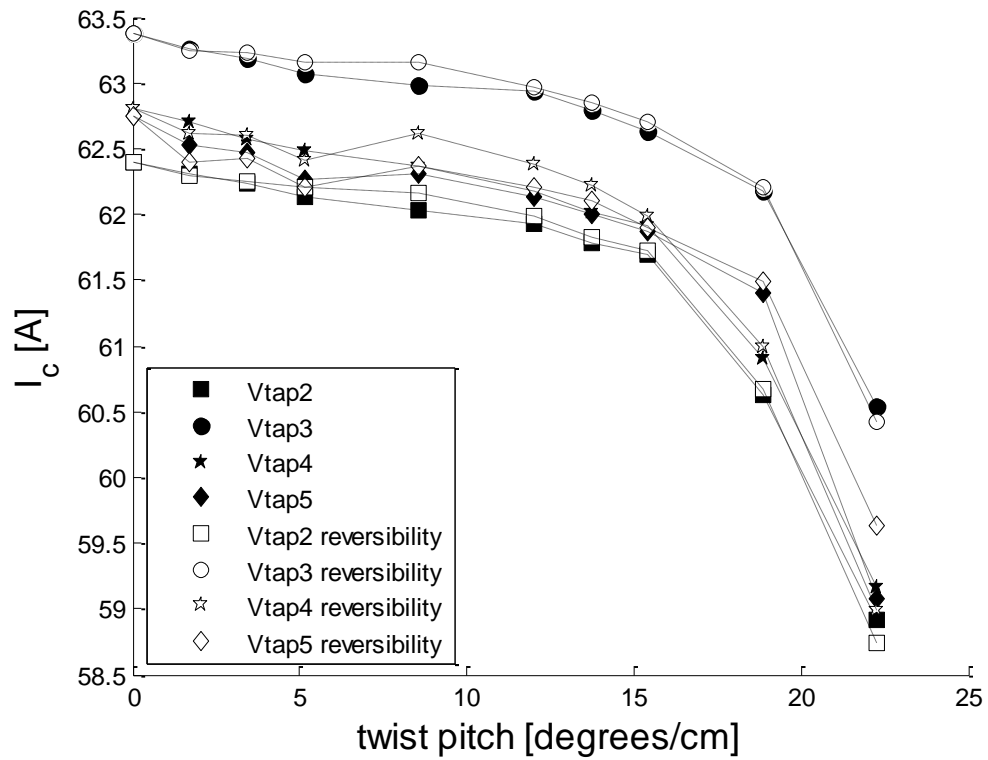


Figure 44: Behaviour of I_c for Bi-2223 tape during pure torsion test.

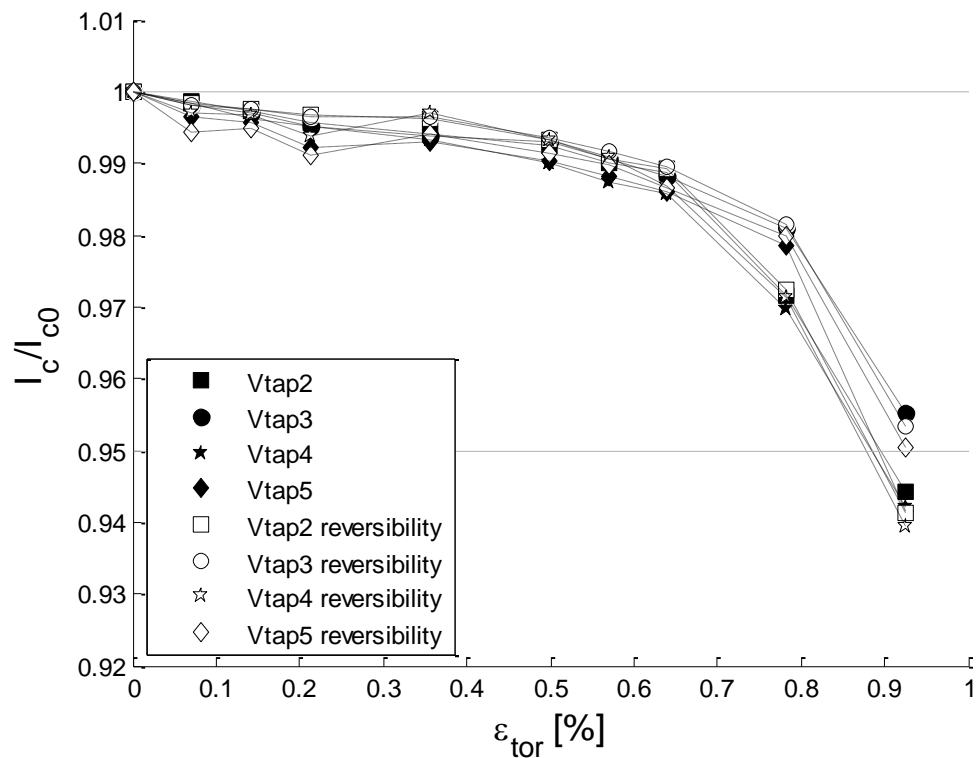


Figure 45: Behaviour of I_c/I_{c0} for Bi-2223 tape during pure torsion test.

We can see that the I_c degradation is still present after removing the strain, with only a very slight recovery for this old Bi-2223 tape. Because of the bad reversibility, in this case $\varepsilon_{c,tor} \approx \varepsilon_{irr,tor} \sim 0.9\%$. The n -index only starts to degrade at around $\varepsilon_{c,tor}$.

It was concluded that the set up and instrumentation worked fine and that ReBCO measurements could begin, with less solder to be used to attach the voltage sensing wires on the sample.

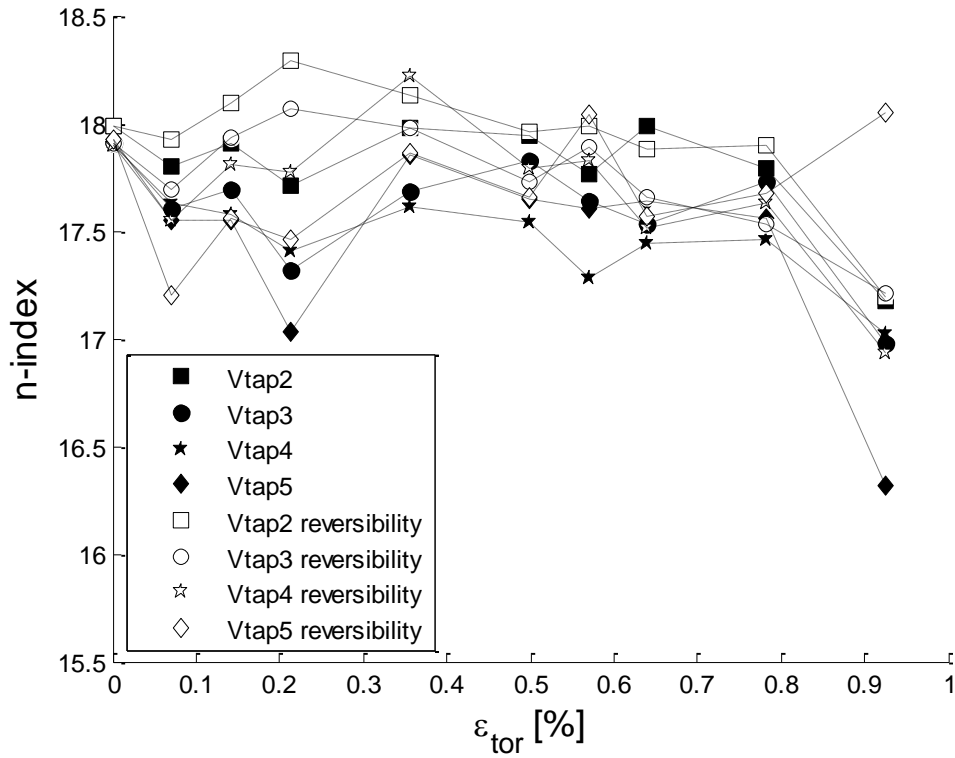


Figure 46: Behaviour of n -index for Bi-2223 tape during pure torsion test.

4.3 ReBCO CC tape measurements

For the ReBCO measurements four different samples (again at 17 cm length) were used with the following measurement scheme:

- Varying torsional strain with fixed (zero) tensile strain: $I_c(T = 77\text{ K}, \varepsilon_{tens} = 0, \varepsilon_{tor})$.
- Varying tensile strain at fixed (zero) torsional strain: $I_c(T = 77\text{ K}, \varepsilon_{tens}, \varepsilon_{tor} = 0)$.
- Varying tensile strain at fixed (300° , $\varepsilon_{tor} \sim 0.3\%$) torsional strain: $I_c(T = 77\text{ K}, \varepsilon_{tens}, \varepsilon_{tor} = 0.3\%)$.
- Varying tensile strain at fixed (480° , $\varepsilon_{tor} \sim 0.5\%$) torsional strain: $I_c(T = 77\text{ K}, \varepsilon_{tens}, \varepsilon_{tor} = 0.5\%)$.

The electric field criterion used for this tape is 10^{-5} Vm^{-1} . The used torsional angles for the last two samples, 300° and 480° , corresponding to $\varepsilon_{tor} \sim 0.31\%$ and $\varepsilon_{tor} \sim 0.50\%$, were chosen based on the results of the torsional strain test; these chosen torsional strains were thought to be high enough to show an significant effect when compared to a pure tensile strain test, yet were thought to be low enough not to cause I_c degradation directly on applying small tensile loads.

4.3.1 Torsional strain test

Measurements were performed on a sample by changing the torsional angle, at fixed tensile load. The increments used are 30° , corresponding to $\Delta\varepsilon_{tens} = 0.031\%$.

After each measurement reversibility was examined by removing the torsional strain; due to limitations of the insert, this was no longer possible after 780° ($46^\circ/cm$) had been reached because the copper current cable, shown in Figure 14, became twisted. This problem was fixed afterwards by smoothing the copper holder surrounding the cable.

Twist pitch was not entirely homogeneous across the sample length, showing up to 13% variation between 180° twist lengths upon examination of the sample when twisted 990° ($58^\circ/cm$) across the entire length.

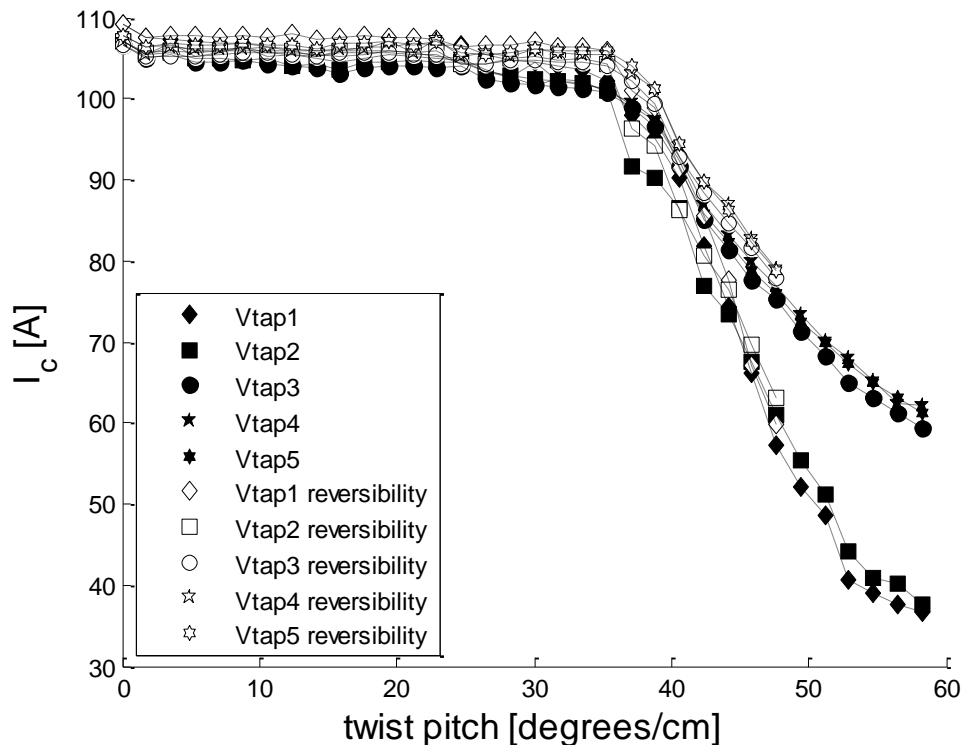


Figure 47: Behaviour of I_c for SCS4050 tape during pure torsion test.

The ReBCO CC tape, with its strong Hastelloy layer, shows a different behaviour than the Bi-2223 tape: up to $\varepsilon_{tor} \sim 0.44\%$, I_c only shows very small degradation ($\sim 2\%$). I_c starts to decrease rather fast after $\varepsilon_{c,tor} \sim 0.58\%$ has been reached. At this point two adjacent voltage taps start to show worse degradation than the other taps, indicating not entirely homogenous behaviour in this region. The reversibility is high up to $\varepsilon_{c,tor}$, after which it also drops steeply.

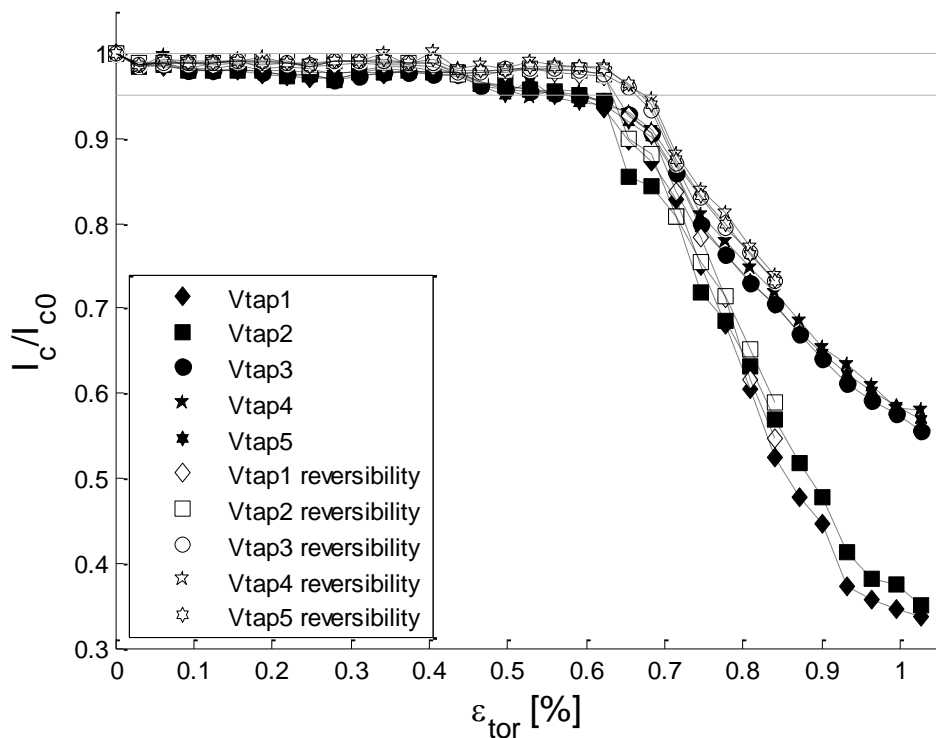


Figure 48: Behaviour of I_c/I_{c0} for SCS4050 tape during pure torsion test.

The n -values for the torsional strain test remain fairly constant for three of the voltage taps, while showing a decrease for the two taps mentioned above starting at $\varepsilon_{c,tor}$. The n -index of voltage tap 4 shows a large spread between adjacent measurement points in both the measurements done under load and with the load removed. Looking at the $V - I$ data, data-points seem to have high enough density (around 8 points/decade) in the electric field decade in which the n -index is fitted using eq. (1). Because this behaviour of voltage tap 4 was also seen in the other measured ReBCO samples, it is highly probable that the spread in n -index originates from the potential measuring circuit of voltage tap 4; it is therefore likely not a characteristic of the sample itself.

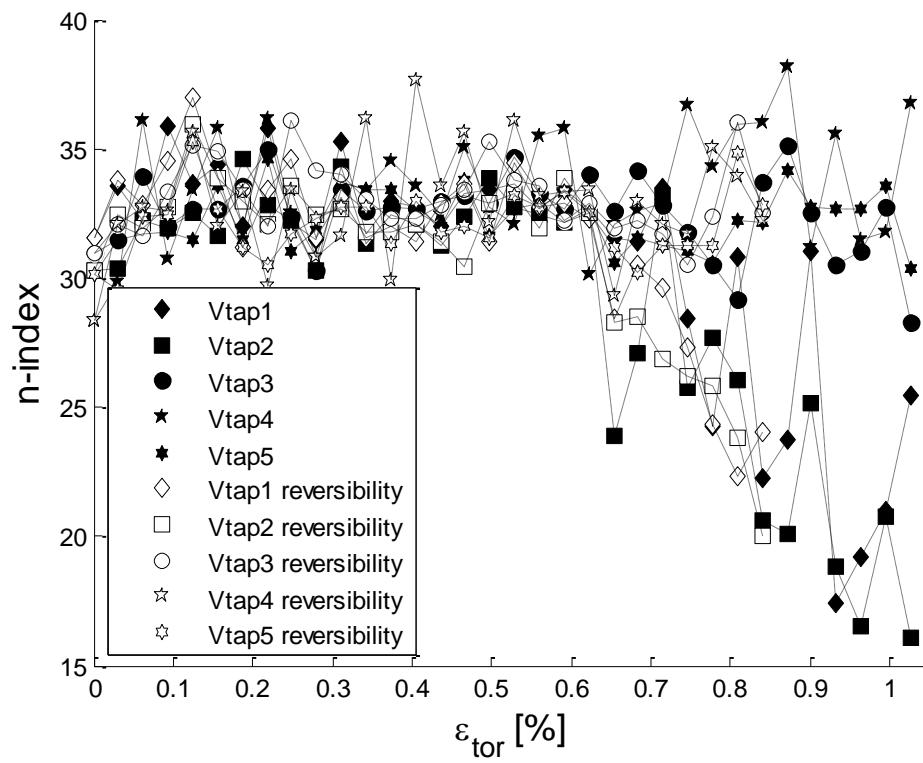


Figure 49: Behaviour of n -index for SCS4050 tape during pure torsion test.

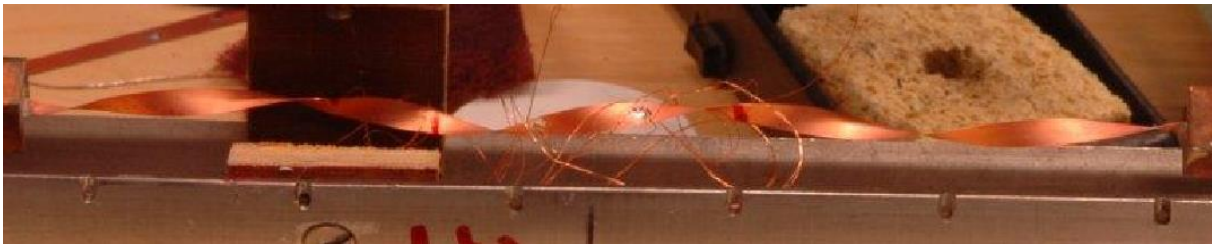


Figure 50: Twisted SCS4050 sample

4.3.2 Tensile strain test

For the second sample the torsional angle was held constant at zero degrees, while the tensile load was changed in 50 N increments. The I_c first becomes slightly higher at small strains, and shows a sharper decline after $\varepsilon_{c,tens} \sim 0.45\%$ has been reached. This value coincides with the value given by the manufacturer, which is also 0.45% [24]. Up to $\varepsilon_{tens} \sim 0.52\%$, reversibility is around 100%; after this it drops sharply ($\varepsilon_{irr,tens} \sim 0.56\%$), with a spread between taps. The n -index again stays fairly constant up to $\varepsilon_{c,tens}$, after which it starts to drop.

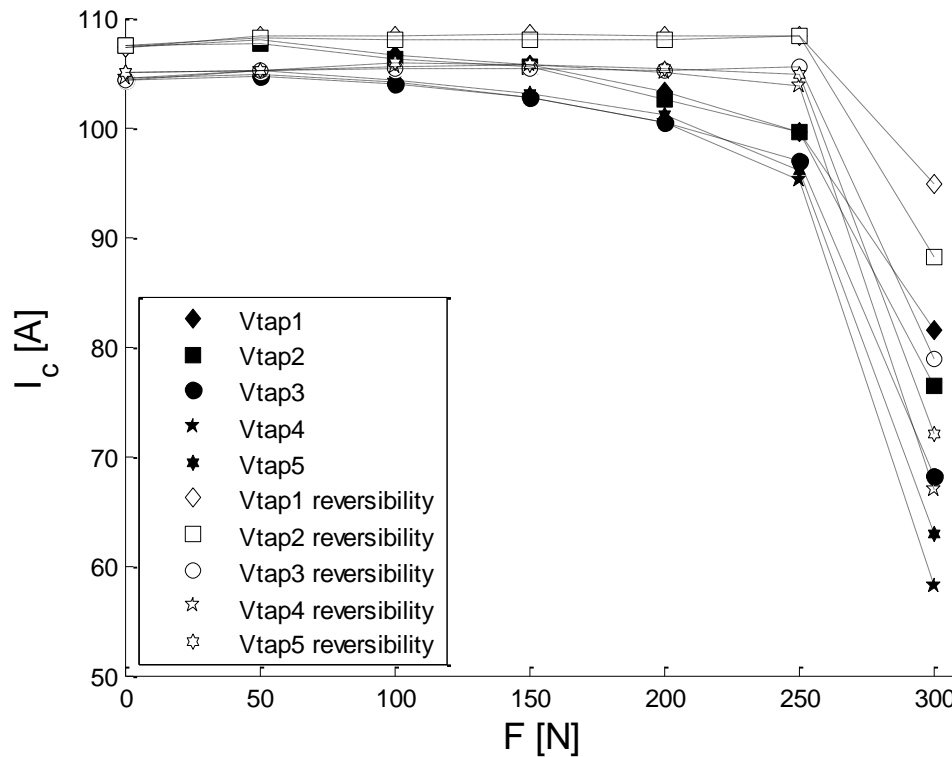


Figure 51: Behaviour of I_c versus applied axial tensile strain for SCS4050 tape during pure tensile test.

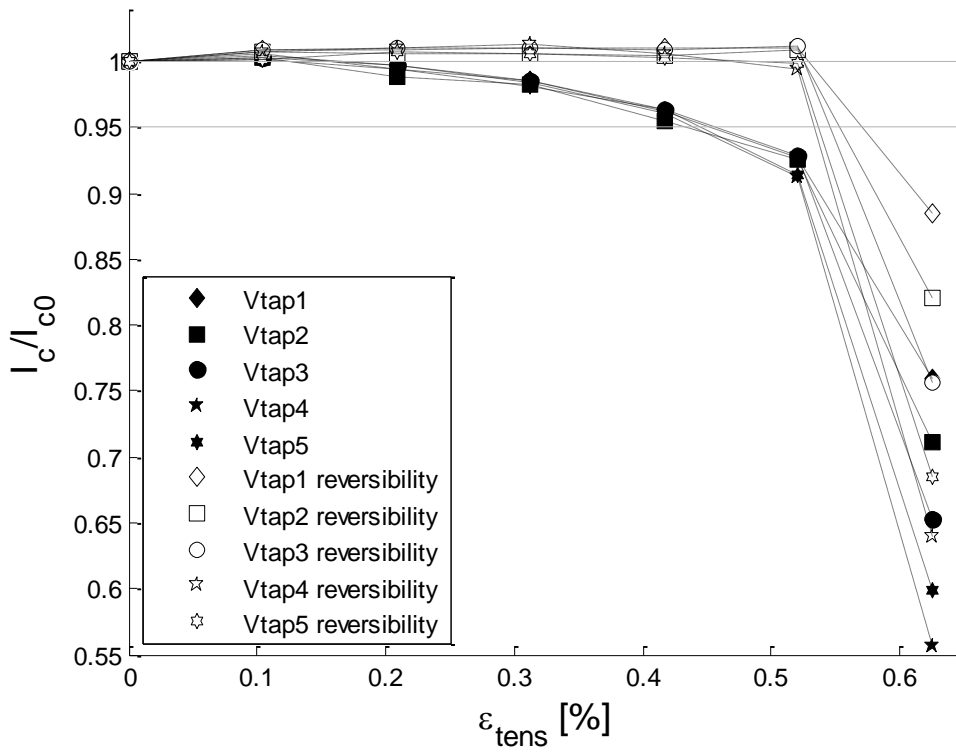


Figure 52: Behaviour of I_c/I_{c0} versus applied axial tensile strain for SCS4050 tape during pure tensile test.

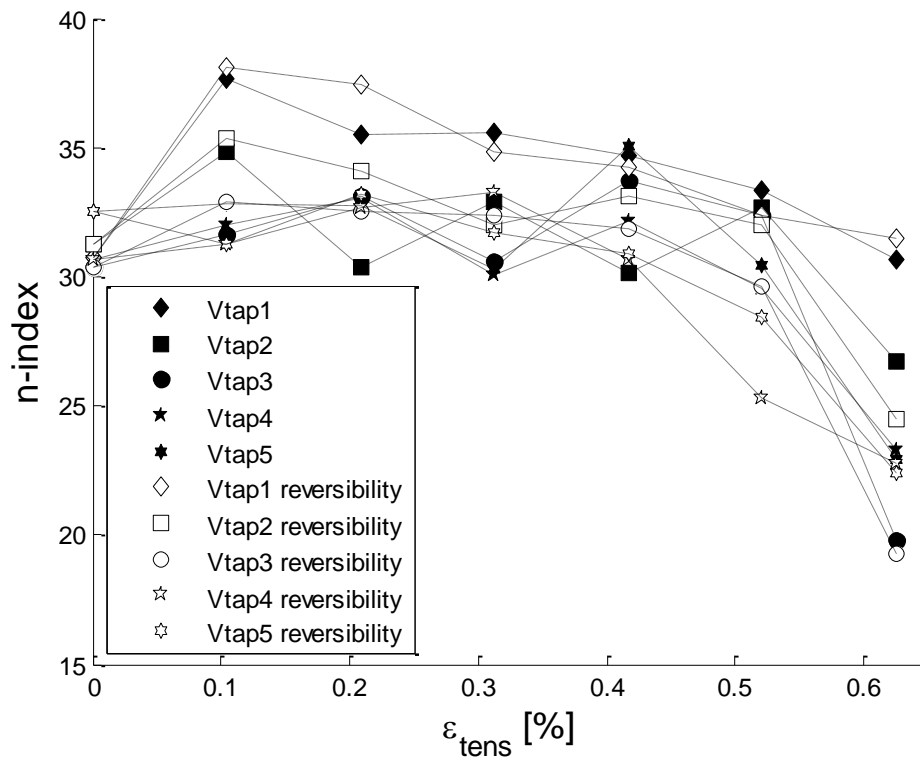


Figure 53: Behaviour of n -index versus applied axial tensile strain for SCS4050 tape during pure tensile test.

4.3.3 Combined strain test #1

For the two combined tests it was decided to use a fixed torsional angle while varying tensile load. The tensile strain was increased in small increments between measurements, with a removal of tensile load between these measurements to test reversibility behaviour. During these reversibility measurements the torsional strain was not removed. For the normalized plots the virgin sample measurement was taken as I_{c0} .

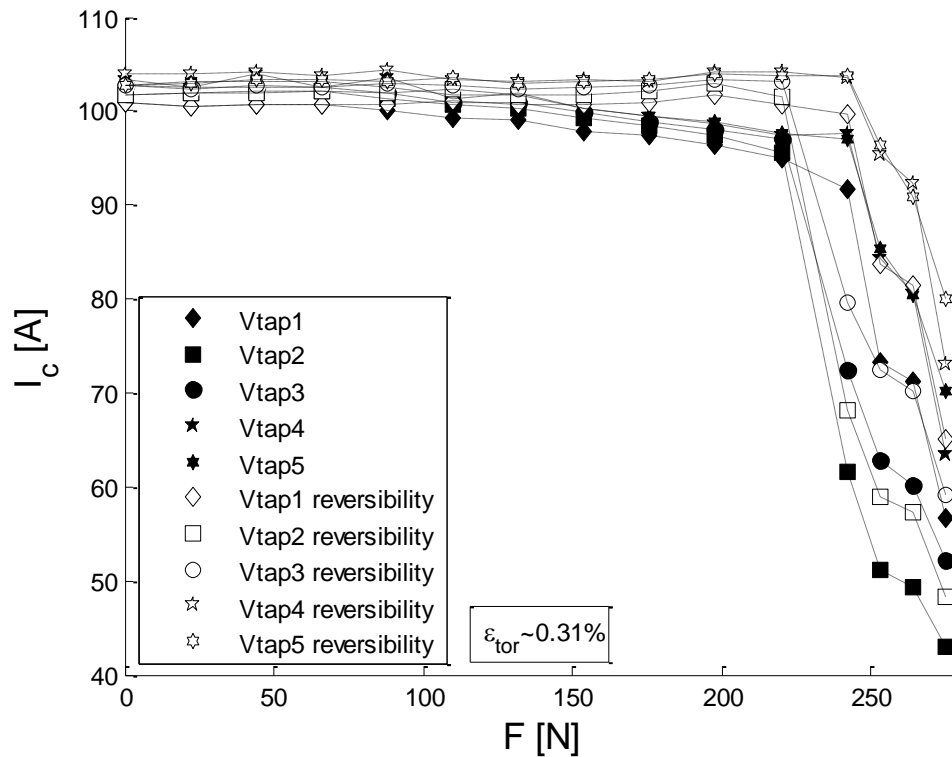


Figure 54: Behaviour of I_c versus applied axial tensile strain for SCS4050 tape during combined test #1.

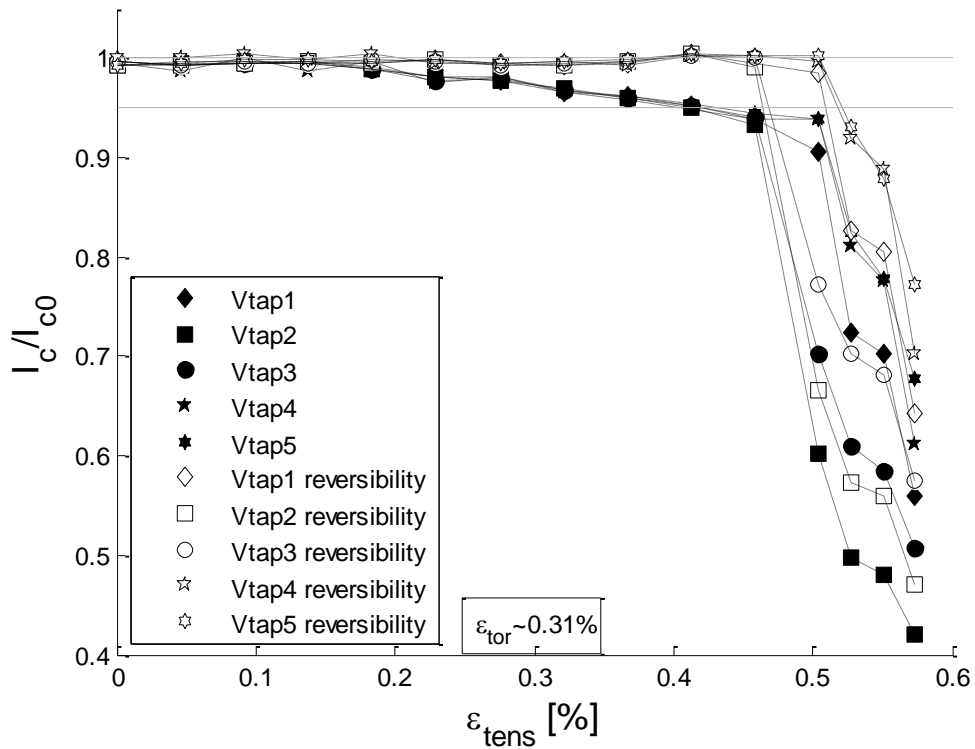


Figure 55: Behaviour of I_c/I_{c0} versus applied axial tensile strain for SCS4050 tape during combined test #1.

The I_c in this first combined strain test ($\epsilon_{tor} \sim 0.31\%$) shows homogeneous behaviour up to $\epsilon_{c,tens} \sim 0.42\%$, after which it shows a large divergence between voltage taps. Up to $\epsilon_{c,tens}$, reversibility is around 100%; higher strain causes a quick collapse and a large spread between taps.

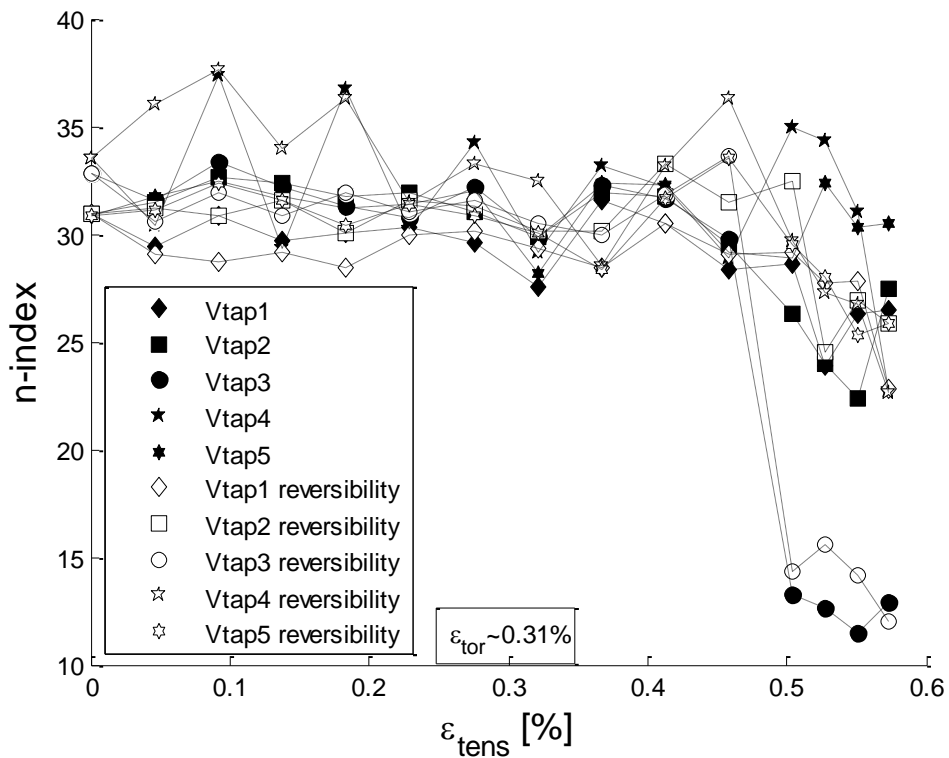


Figure 56: Behaviour of n -index versus applied axial tensile strain for SCS4050 tape during combined test #1.

The n -values in this combined strain test stay fairly constant up to $\varepsilon_{c,tens}$; a slow decrease can be observed at higher strains, with one tap dropping very sharply as an exception.

4.3.4 Combined strain test #2

In the second combined strain test, a torsional angle of 480° , corresponding to $\varepsilon_{tor} \sim 0.50\%$ was applied to the sample. A tensile load test was performed in the same way as in the first combined test.

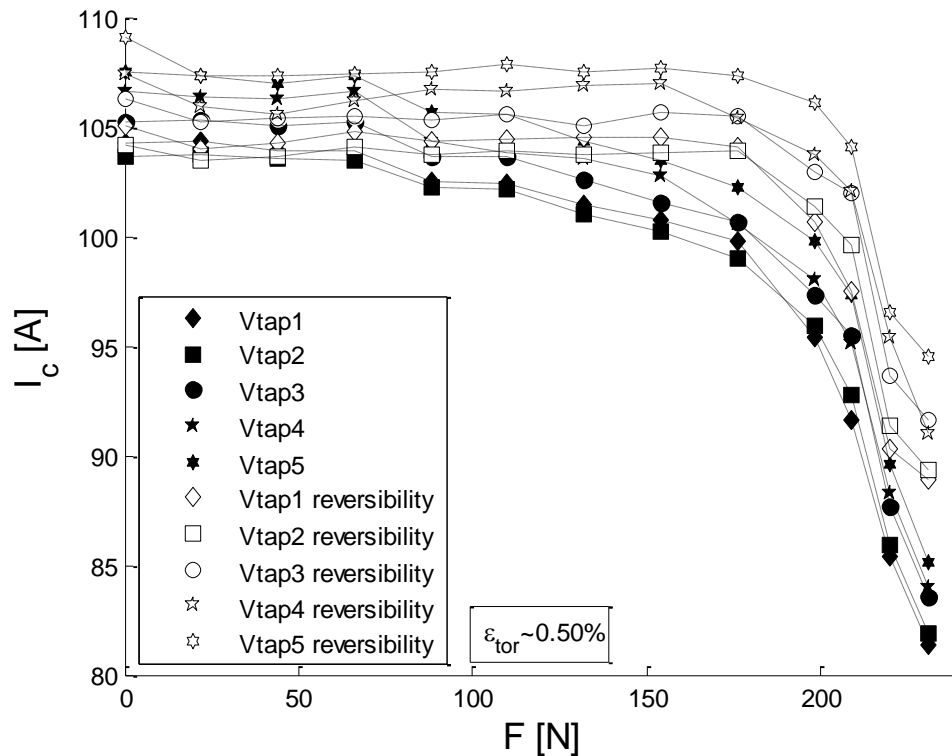


Figure 57: Behaviour of I_c versus applied axial tensile strain for SCS4050 during combined test #2.

In Figure 58 we can observe a gradual decrease in I_c starting around $\varepsilon_{tens} \sim 0.1\%$. The critical strain can be found at $\varepsilon_{tens} \sim 0.34\%$; higher strain make for a rapid decline in I_c . Reversibility is constant up to $\varepsilon_{tens} \sim 0.36\%$, showing a steep drop at higher strain, with $\varepsilon_{irr,tens} \sim 0.43\%$.

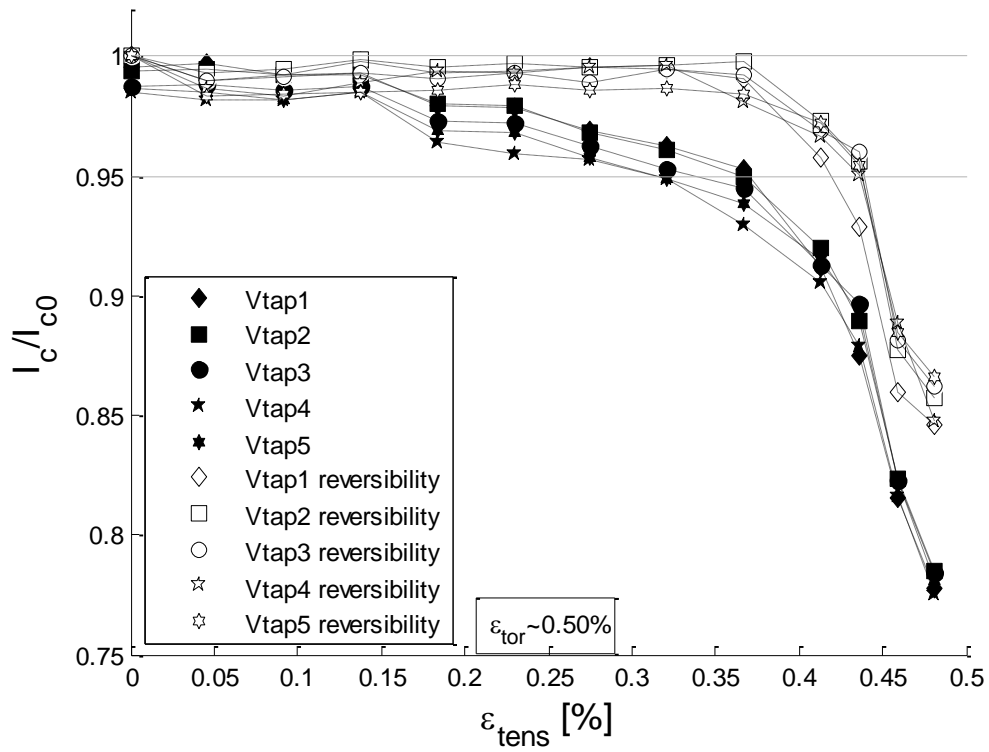


Figure 58: Behaviour of I_c/I_{c0} versus applied axial tensile strain for SCS4050 tape during combined test #2.

The n -values again show some strange oscillations for voltage tap #4. One can also observe some deviation in the higher strain regime, though measurement point density is the same as in other measurements at around eight points per decade.

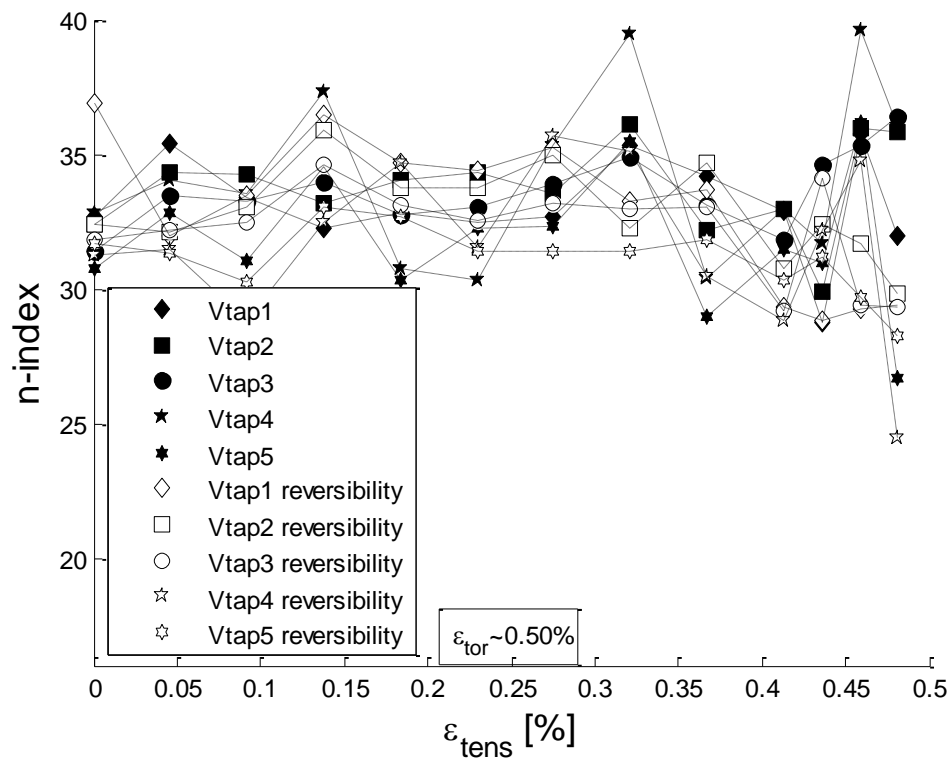


Figure 59: Behaviour of n -index versus applied axial tensile strain for SCS4050 tape during combined test #2.

4.3.5 Comparison of ReBCO measurements

In Figure 60 the I_c -results for the five voltage taps are averaged and plotted together for the four different ReBCO measurements. Voltage tap 4 data was not used for the average n -index in Figure 61 because of the previously discussed spread in adjacent data points.

From these plots a general trend becomes visible for the reversibility: reversibility is very high at low tensile strains despite the torsional strain present. A small constant degradation can be seen however, as a result of the torsional strain still present during reversibility measurements. After the strain has reached $\varepsilon_{c,tens}$ the irreversibility starts to increase quickly.

For this SCS4050 tape, moderate combined torsional and tensile strains do not seem a big issue in cases where the strains are no longer present during operation. When the torsional strain is increased from zero to 0.5%, the irreversibility limit decreases from $\varepsilon_{tens} \sim 0.55\%$ to around 0.43%. Majkic *et al* found similar results on a ReBCO CC tape with Hastelloy substrate, and noted that the drop in I_c becomes more smoothly at higher torsional strains compared to the relatively sudden drop seen at lower applied torsional strains [9].

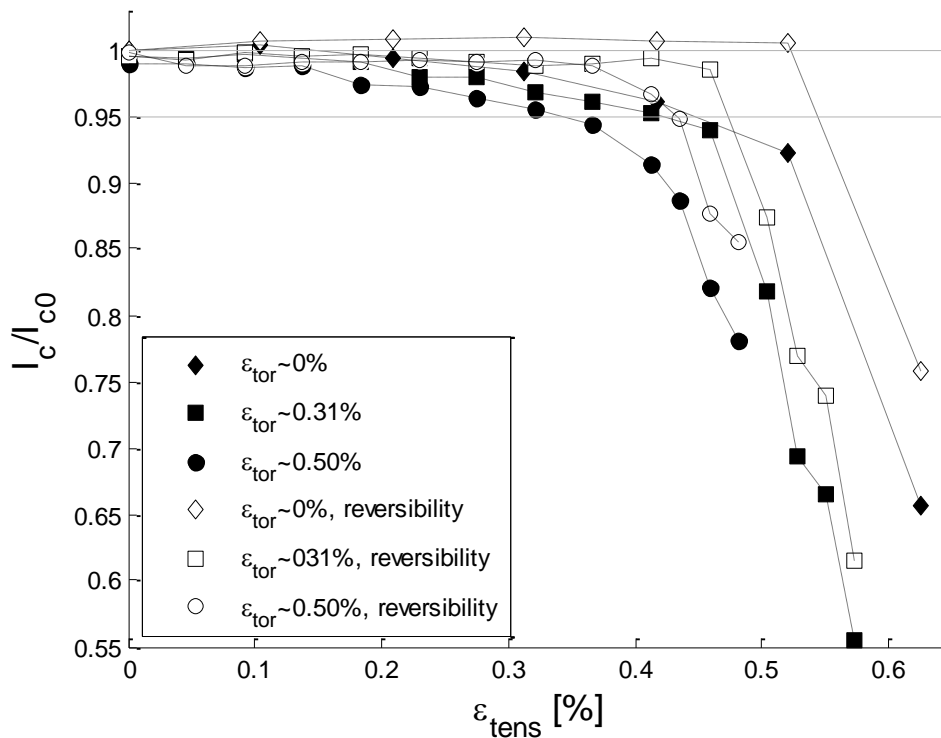


Figure 60: Comparison of I_c/I_{c0} versus applied axial tensile strain from different measurements on SCS4050 tape.

The n -index is more or less constant up to $\varepsilon_{tens} \sim 0.4\%$, with a gradual decrease at higher tensile strains. The applied torsional strain does seem to have some influence on the n -index in this measurement although similar tendency is found as for I_c . Spread between the curves is thought to be the result from inhomogeneous characteristics of the used SCS4050 tape or from changing strain distributions with varying load combinations.

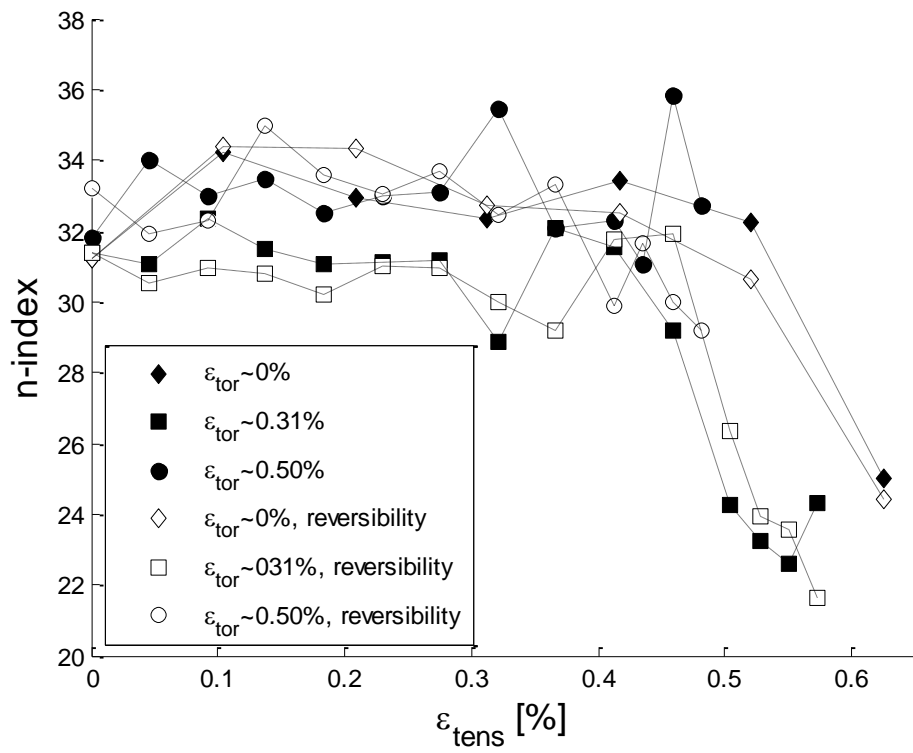


Figure 61: Comparison of n -index versus applied axial tensile strain from different measurements on SCS4050 tape.

Chapter 5: Conclusion

An insert for applying combined torsional and tensile strain on superconducting samples is now working properly.

The following measurements investigating the effects of torsional and tensile strain on the electromagnetic properties of superconductors were performed:

- *Varying torsional strain at fixed (zero) tensile strain on a steel reinforced Bi-2223 tape.*
The Bi-2223 tape showed a relatively high $\varepsilon_{c,tor} \sim 0.9\%$, but reversibility for this tape was found to be almost non-existent. This means that any torsional strain will permanently damage the Bi-2223 tape and therefore should be avoided.
- *Varying torsional strain with fixed (zero) tensile strain on a CC ReBCO tape.*
The ReBCO tape shows a different behaviour than the Bi-2223 tape: the critical torsional strain has a lower value, $\varepsilon_{c,tor} \sim 0.58\%$, and I_c starts to decrease rather fast at higher strains. Starting from $\varepsilon_{c,tor}$ two voltage taps start to show worse degradation than the other taps, indicating not entirely homogenous behaviour in this region. The reversibility is high up to $\varepsilon_{c,tor}$ after which it also drops steeply.
- *Varying tensile strain at fixed (zero) torsional strain on a CC ReBCO tape.*
The I_c first becomes slightly higher at small strains; this is probably due to the relaxation of the compression that occurs during cooling. The critical current shows a sharp decline after $\varepsilon_{c,tens} \sim 0.45\%$ has been reached, which is also the value given by the manufacturer. Up to $\varepsilon_{tens} \sim 0.52\%$, reversibility is 100%; After this it drops very sharply ($\varepsilon_{irr,tens} \sim 0.56\%$).
- *Varying tensile strain at fixed ($\varepsilon_{tor} \sim 0.3\%$) torsional strain on a CC ReBCO tape.*
The I_c in the first combined strain test shows homogeneous behaviour up to $\varepsilon_{c,tens} \sim 0.42$, after which it shows a large divergence between voltage taps. Up to $\varepsilon_{c,tens}$, reversibility is around 100%; higher strain causes a quick collapse and a large spread between taps.
- *Varying tensile strain at fixed ($\varepsilon_{tor} \sim 0.5\%$) torsional strain for on a CC ReBCO tape.*
The critical strain in the second combined strain test can be found at $\varepsilon_{tens} \sim 0.34\%$; higher strain causes a rapid decline in I_c . Reversibility is constant up to $\varepsilon_{tens} \sim 0.36\%$, showing a steep drop at higher strain, with $\varepsilon_{irr,tens} \sim 0.43\%$.

For the ReBCO CC tape in general the homogeneity of the I_c across taps is good up to around $\varepsilon_{c,tens}$, after which divergent behaviour can be observed. Reversibility is very high and starts to drop sharply around $\varepsilon_{c,tens}$. The n -index shows a slow decrease at higher strain, this decrease is still present after strain has been removed.

Simulations in COMSOL using the finite element method (FEM) provided stress profiles in the tape resulting from torsional strain, valid in the elastic stress-strain region. From comparing the stress to yield stress across the different materials in the tape, it can be concluded that the copper layer is the first to show plastic deformation, followed by the silver layer. To reach the aim of the modeling work, a quantitative analysis of the strain distribution in the ReBCO layer, more work is needed.

It is probable that damage resulting from tensile strain in the ReBCO CC tape will occur because of the formation of cracks at localized sites, while damage occurring from torsional strain occurs more gradually because cracks can propagate more uniformly along the tape and the torsional strain is a peak strain, only present at the edges of the ReBCO layer. This explains the more sudden I_c degradation under tensile strain compared to torsional strain.

A better understanding of electro-mechanical properties of the ReBCO CC tape could be obtained by microscopy on the surfaces of the different layers of the tape, after the tape has been subjected to strain. By using different combinations of tensile and torsional strain, one will get an idea of the damaging of the ReBCO layer.

References

1. *High Energy Physics*. [cited 2013 01/24]; Available from: <http://www.hep.ucl.ac.uk/undergrad-projects/3rdyear/PPguide/cool.htm>.
2. *Magnets*. [cited 2013 01/24]; Available from: <http://www.iter.org/mach/magnets>.
3. Hawsey, R.A. and D.K. Christen, *Progress in research, development, and precommercial deployment of second generation HTS wires in the USA*. Physica C: Superconductivity and its applications, 2006. **445-448**: p. 488-495.
4. Bansal, G., et al. *High-temperature superconducting coil option for the fusion reactor FFHR and the development of indirectly-cooled HTS conductors*. in *TC/ISHW2007*. 2007.
5. Shin, H.-S., J.R.C. Dizon, and T.-H. Kim, *Critical current degradation behavior in YBCO coated conductors under torsional strain*. IEEE Transactions on Applied Superconductivity, 2007. **17**(2): p. 3274-3277.
6. Sugano, M., et al., *Intrinsic strain effect on critical current and its reversibility for YBCO coated conductors with different buffer layers*. Superconductor Science and Technology, 2005. **18**(3): p. 369-372.
7. Cheggour, N., et al., *Reversible axial-strain effect in Y-Ba-Cu-O coated conductors*. Superconductor Science and Technology, 2005. **18**(12): p. S319-S324.
8. Shin, H.-S., et al., *I_c degradation behavior in Bi-2223 superconducting tapes under torsional deformation*. Physica C: Superconductivity, 2003. **392-396**: p. 1162-1166.
9. Majkic, G., R.J. Mensah, and V. Selvamanickam, *Electromechanical Behavior of IBAD/MOCVD YBCO Coated Conductors Subjected to Torsion and Tension Loading*. IEEE Transactions on Applied Superconductivity, 2009. **19**(3): p. 3003-3008.
10. Kamerlingh Onnes, H., *Further experiments with liquid helium. D. On the change of electric resistance of pure metals at very low temperatures, etc. V. The disappearance of the resistance of mercury*. KNAW, proceedings, 1911. **124c**.
11. Goyal, A., *Second-Generation HTS Conductors*2005, Norwell, Massachusetts: Kluwer Academic Publishers.
12. Kakani, S.L., *Superconductivity*2009, Tunbridge Wells, Kent: Ashan LTD.
13. Nelson, E. *Stress and Strain*. 1999 [cited 2013 04/22]; Available from: www.mbari.org/staff/conn/botany/methods/methods/stress.htm.
14. Roylance, D. *Stress-Strain Curves*. 2001 [cited 2013 03/05]; Available from: web.mit.edu/course/3/3.11/www/modules/ss.pdf
15. Meyers, M.A. and K.K. Chawla, *Mechanical Behavior of Materials*2009, Cambridge: Cambridge University Press.
16. Hellstrom, E.E., *High Temperature Superconducting Materials Science and Engineering*. 1st ed1995: Elsevier Science Ltd.
17. Motowidlo, L.R., G. Galinski, and P. Haldar, in *Materials Research Society Spring Meeting*1993: San Francisco.
18. Weissend, J.G., *Handbook of Cryogenic Engineering*1998, Philadelphia: Taylor & Francis.
19. Wijers, H., *High-temperature superconductores in high-field magnets*, in *TNW2009*, University of Twente: Enschede.
20. Petrucci, R., *General Chemistry: Principles & Modern Applications*. 9th ed2007: Prentice Hall.
21. Passerini, R. and M. Dhallé, *The influence of thermal precompression on the mechanical behaviour of Ag-sheathed (Bi,Pb)2223 tapes with different matrices*. Physica C: Superconductivity, 2002. **371**(3): p. 173-184.
22. ten Haken, B., A. Beuink, and H.J. ten Kate, *Small and repetitive axial strain reducing the critical current in BSCCO/Ag superconductors*. IEEE Transactions on Applied Superconductivity, 1997. **7**(2): p. 2034-2038.
23. Hazelton, D., *Application of SuperPower 2G HTS Wire to High Field Devices*, in *MT22 Conference*2011: Marseille.

24. *SuperPower 2G HTS wire specifications*. [cited 2013 04/22]; Available from: http://www.superpower-inc.com/system/files/SP_2G+Wire+Spec+Sheet_for+web_0509.pdf.
25. *SuperPower 2G HTS wire specifications*. [cited 2013 04/20]; Available from: http://www.superpower-inc.com/system/files/SP_2G+Wire+Spec+Sheet_for+web_2012FEC_v2_1.pdf.
26. *HASTELLOY C-276 alloy information*. 2001 [cited 2013 04/22]; Available from: <http://www.haynesintl.com/HASTELLOYC276Alloy/HASTELLOYC276AlloyPF.htm>.
27. Hazelton, D. *High-Temperature Superconducting (HTS) Wire And Applications*. 2010.
28. Joseph, G. and K.J.A. Kundig, *Copper: Its Trade, Manufacture, Use and Environmental Status* 1999: ASM International.
29. *The International Annealed Copper Standard*. [cited 2013 04/22]; Available from: www.ndt-ed.org/GeneralResources/IACS/IACS.htm.
30. Yen, C. and T. Caulfield, *Creep of copper at cryogenic temperatures*. Cryogenics, 1984.
31. *C-276 specification sheet*. [cited 2013 04/22]; Available from: <http://www.agcheattransfer.com/wp-content/uploads/Specialty-metals-INCONEL-alloy-C276-specification-sheet.pdf>.
32. Sugano, M., *Tensile fracture behaviour of RE-123 coated conductors induced by discontinuous yielding in Hastelloy C-276 substrate*. Superconductor Science and Technology, 2005. **18**(12): p. 344-350.
33. *Hastelloy C-276 technical data*. [cited 2013 04/22]; Available from: <http://www.hightempmetals.com/techdata/hitempHastC276data.php>.
34. Goyal, A., W.C. Oliver, and P.D. Funckenbusch, *Mechanical properties of highly aligned YBa₂Cu₃O_{7-δ} effect of Y₂BaCuO_x particles*. Physica C: Superconductivity, 1001. **183**(4-6): p. 221-233.
35. Yamada, Y., J. Kawashima, and J.-G. Wen, *Evaluation of thermal expansion coefficient of twinned YBa₂Cu₃O₇₋₈ film for prediction of crack formation on various substrates*. Japanese Journal of Applied Physics, 2000. **39**(3A): p. 1111-1115.
36. Nuchteren, J.v. *Normal Zone Propagation in a YBCO Superconducting Tape*. 2012.
37. Smith, D.R. and F.R. Fickett, *Low temperature properties of silver*. J. Res. Natl. Inst. Stand. Tech., 1995. **100**(119).
38. de Weck, O. and I. Yong Kim. *Finite Element Method*. 2004 [cited 2013 06/14]; Available from: http://web.mit.edu/16.810/www/16.810_L4_CAE.pdf.
39. Budynas, R.G. and J.K. Nisbett, *Shigley's Mechanical Engineering Design*. 8th ed 2008, New York: McGraw-Hill.
40. Beardmore, R. *Torsion*. 2010 [cited 2013 04/22]; Available from: http://www.roymech.co.uk/Useful_Tables/Torsion/Torsion.html.
41. Meade, C. and R. Jeanloz, *Yield Strength of MgO to 40 GPa*. Journal of Geophysical Research, 1988. **93**(B4): p. 3261-3269.

Appendix: COMSOL settings

In the pictures below one can find the settings used in the COMSOL simulation.

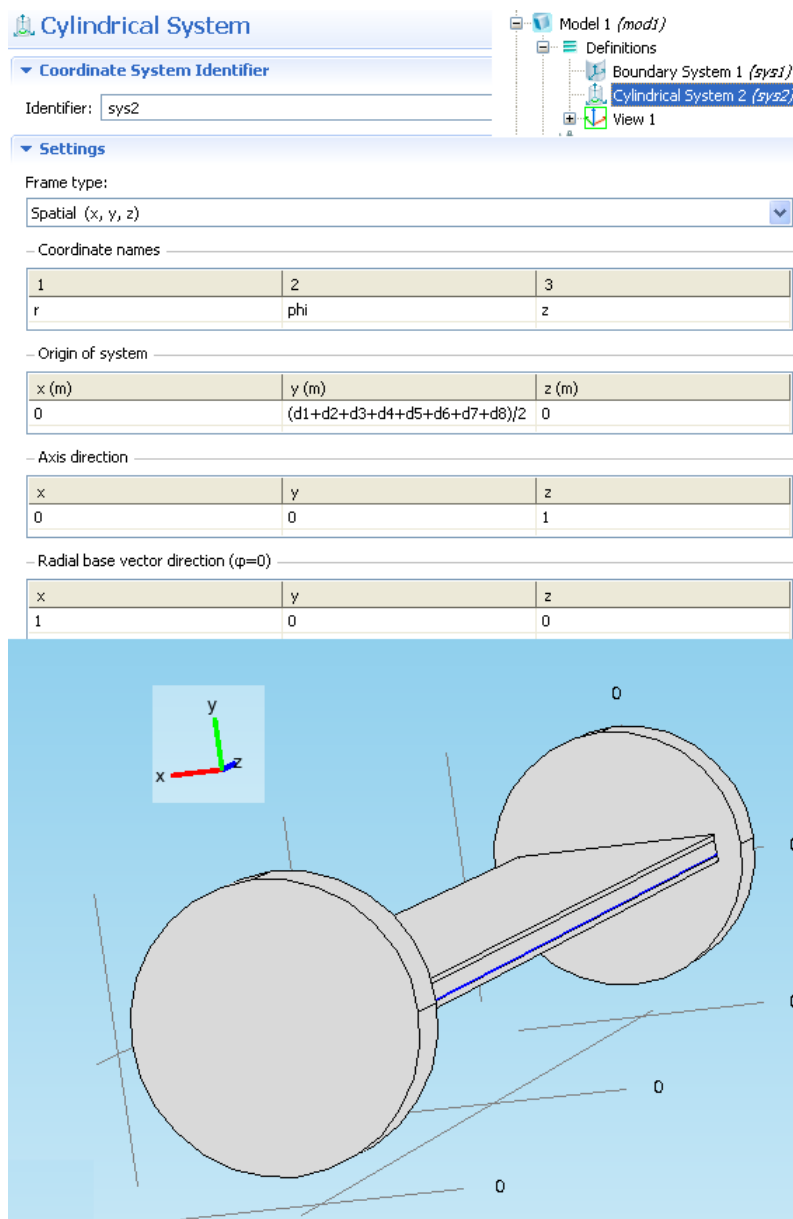


Figure 62: COMSOL cylindrical coordinate system.

Property	Name	Value	Unit
Density	rho	8940[kg/m ³]	kg/m ³
Young's modulus	E	136e9[Pa]	Pa
Poisson's ratio	nu	0.34	1

Cu

Property	Name	Value	Unit
Density	rho	8890	kg...3
Young's modulus	E	216e9[Pa]	Pa
Poisson's ratio	nu	0.307	1

Hastelloy

Property	Name	Value	Unit
Density	rho	10630	kg...3
Young's modulus	E	89.82e9[Pa]	Pa
Poisson's ratio	nu	0.364	1

Ag

Property	Name	Value	Unit
Poisson's ratio	nu	0.3	1
Density	rho	6300[kg/m ³]	kg/m ³
Young's modulus	E	157e9[Pa]	Pa

YBCO

Figure 63: COMSOL material parameters.

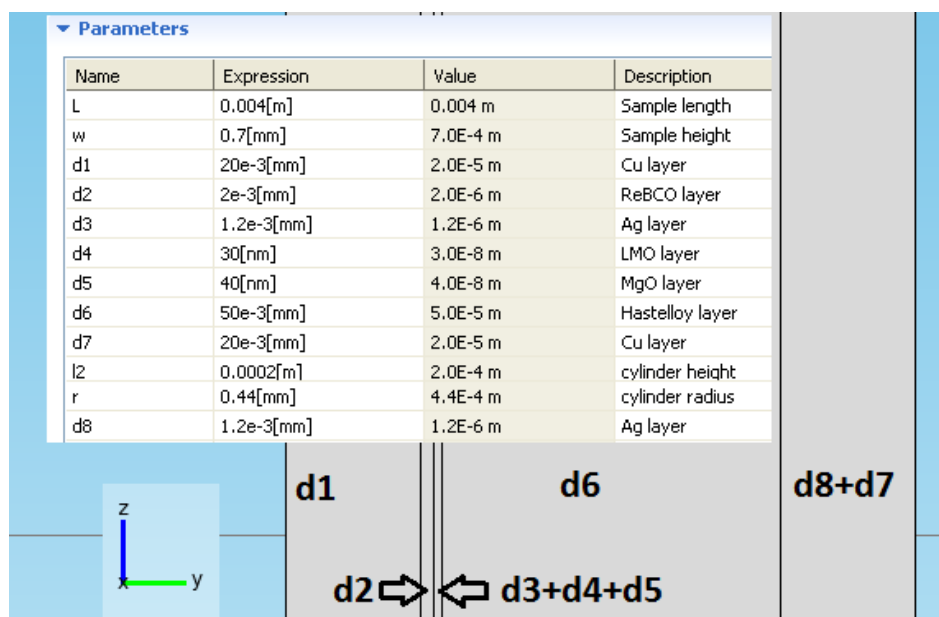


Figure 64: COMSOL geometry parameters.

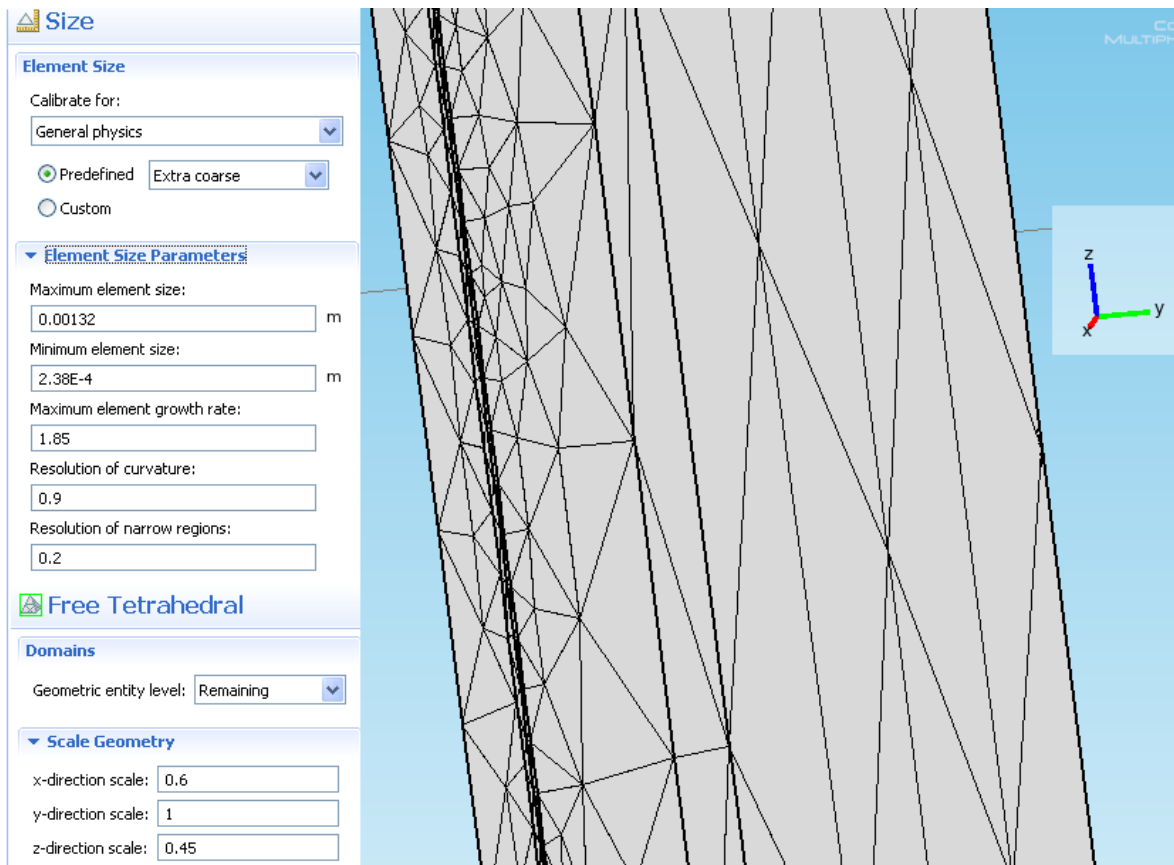


Figure 65: COMSOL mesh settings.

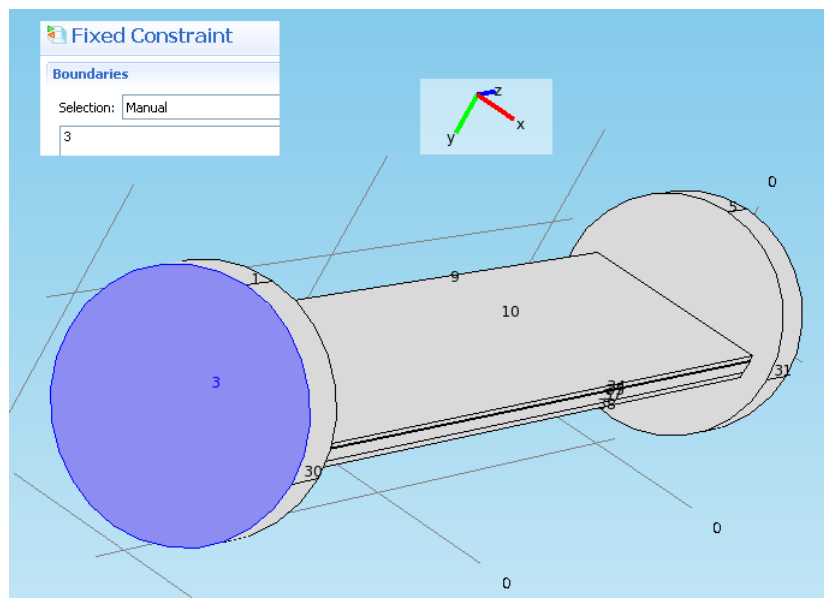


Figure 66: COMSOL fixed end.

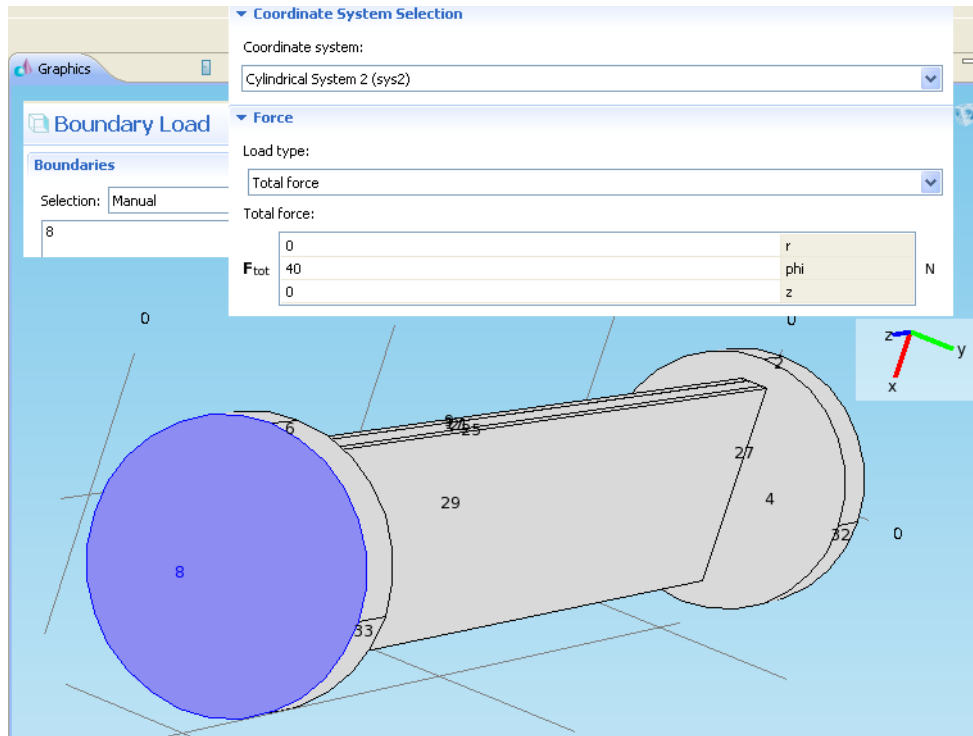


Figure 67: COMSOL boundary load.